

## The Pan-STARRS Moving Object Processing System

Larry Denneau<sup>1</sup> (denneau@ifa.hawaii.edu), Robert Jedicke<sup>1</sup>, Tommy Grav<sup>2</sup>, Mikael Granvik<sup>3</sup>, Jeremy Kubica<sup>4</sup>, Andrea Milani<sup>5</sup>, Peter Vereš<sup>1</sup>, Richard Wainscoat<sup>1</sup>, Daniel Chang<sup>1</sup>, Francesco Pierfederici<sup>6</sup>, N. Kaiser<sup>1</sup>, K. C. Chambers<sup>1</sup>, J. N. Heasley<sup>1</sup>, Eugene. A. Magnier<sup>1</sup>, P. A. Price<sup>7</sup>, Jonathan Myers<sup>8</sup>, Jan Kleyna<sup>1</sup>, Henry Hsieh<sup>1</sup>, Davide Farnocchia<sup>5,9</sup>, Chris Waters<sup>1</sup>, W. H. Sweeney<sup>1</sup>, Denver Green<sup>1</sup>, Bryce Bolin<sup>1</sup>, W. S. Burgett<sup>1</sup>, J. S. Morgan<sup>1</sup>, John L. Tonry<sup>1</sup>, K. W. Hodapp<sup>1</sup>, Serge Chastel<sup>1</sup>, Steve Chesley<sup>9</sup>, Alan Fitzsimmons<sup>10</sup>, Matthew Holman<sup>11</sup>, Tim Spahr<sup>12</sup>, David Tholen<sup>1</sup>, Gareth V. Williams<sup>12</sup>, Shinsuke Abe<sup>13</sup>, J.D. Armstrong<sup>1</sup>, Terry H. Bressi<sup>14</sup>, Robert Holmes<sup>15</sup>, Tim Lister<sup>16</sup>, Robert S. McMillan<sup>14</sup>, Marco Micheli<sup>1</sup>, Eileen V. Ryan<sup>17</sup>, William H. Ryan<sup>17</sup>,  
James V. Scotti<sup>14</sup>

Received \_\_\_\_\_; accepted \_\_\_\_\_

57 Pages, 26 Figures, 13 Tables

---

<sup>1</sup>Institute for Astronomy, University of Hawai‘i, 2680 Woodlawn Dr., Honolulu, HI 96822

<sup>2</sup>Johns Hopkins University, Baltimore, MD

<sup>3</sup>Department of Physics, P.O. Box 64, 00014 University of Helsinki, Finland

<sup>4</sup>Google, Inc.

<sup>5</sup>University of Pisa, Pisa, Italy

<sup>6</sup>Space Telescope Science Institute, 3700 San Martin Dr., Baltimore, MD 21218

<sup>7</sup>Department of Astrophysical Sciences, Princeton University, Princeton, NJ 08544

<sup>8</sup>University of Arizona, Tucson, AZ

<sup>9</sup>Jet Propulsion Laboratory, Pasadena, CA

<sup>10</sup>Astrophysics Research Centre, School of Mathematics and Physics, Queen’s University  
Belfast, Belfast, BT7 1NN, UK

<sup>11</sup>Harvard-Smithsonian Center for Astrophysics, 60 Garden St., Cambridge, MA 02138

<sup>12</sup>Smithsonian Astrophysical Observatory, Cambridge, MA

<sup>13</sup>Institute of Astronomy, National Central University, Taiwan

<sup>14</sup>Lunar & Planetary Laboratory, University of Arizona, Tucson, AZ

<sup>15</sup>Astronomical Research Institute, 7644 NCR 1800E, Charleston, IL 61920

<sup>16</sup>Las Cumbres Observatory Global Telescope Network, Inc., 6740 Cortona Dr. Suite 102,  
Santa Barbara, CA 93117

<sup>17</sup>Magdalena Ridge Observatory, New Mexico Tech, 801 Leroy Pl., Socorro, NM 87801

## ABSTRACT

We describe the Pan-STARRS Moving Object Processing System (MOPS), a modern software package that produces automatic asteroid discoveries and identifications from catalogs of transient detections from next-generation astronomical survey telescopes. MOPS achieves  $> 99.5\%$  efficiency in producing orbits from a synthetic but realistic population of asteroids whose measurements were simulated for a Pan-STARRS4-class telescope. Additionally, using a non-physical grid population, we demonstrate that MOPS can detect populations of currently unknown objects such as interstellar asteroids.

MOPS has been adapted successfully to the prototype Pan-STARRS1 telescope despite differences in expected false detection rates, fill-factor loss and relatively sparse observing cadence compared to a hypothetical Pan-STARRS4 telescope and survey. MOPS remains highly efficient at detecting objects but drops to 80% efficiency at producing orbits. This loss is primarily due to configurable MOPS processing limits that are not yet tuned for the Pan-STARRS1 mission.

The core MOPS software package is the product of more than 15 person-years of software development and incorporates countless additional years of effort in third-party software to perform lower-level functions such as spatial searching or orbit determination. We describe the high-level design of MOPS and essential subcomponents, the suitability of MOPS for other survey programs, and suggest a road map for future MOPS development.

*Subject headings:* Surveys:Pan-STARRS; Near-Earth Objects; Asteroids

## 1. Introduction

As with most scientific endeavors, the history of asteroid and comet studies depicts an exponential increase in the rate of discovery since the identification of Ceres by Piazzi more than 200 years ago. This work describes the next step in the evolution of asteroid surveys — an integrated, end-to-end moving object processing system (MOPS) for the Panoramic Survey Telescope and Rapid Response System (Pan-STARRS Kaiser et al. 2002; Kaiser 2004; Hodapp et al. 2004). The system’s prototype telescope (PS-1) employs a 1.4 gigapixel camera able to detect asteroids and comets faster than ever before.

The first asteroids were discovered serendipitously and laboriously by eye until the dedicated photographic surveys of the 1950s and 1960s like the Yerkes-McDonald (Kuiper et al. 1958) and Palomar Leiden Surveys (van Houten et al. 1970). The photographic surveys required a major effort due to the need for human ‘blinking’ of the images to identify the moving objects. The realization in the early 1980s by Alvarez et al. (1980) that the extinction of the dinosaurs  $\sim 65$  million years ago was precipitated by the impact of a large asteroid or comet with the Earth stimulated enhanced funding for wide field asteroid surveys. While those surveys identified many asteroids and comets that may eventually strike the Earth, only one object has been discovered that actually hit the Earth — 2008 TC<sub>3</sub> (*e.g.* Jenniskens et al. 2009; Boattini et al. 2009).

The photographic searches leveraged decades of experience in wide field astronomical surveying but Spacewatch (Gehrels 1991; McMillan 2007) spearheaded the first use of CCDs in asteroid surveys. In the beginning, the small CCDs of the time limited the success of this search program but the asteroid discovery rate improved dramatically when they obtained a high quantum efficiency 2K $\times$ 2K CCD with an  $\sim 30$  arcmin field of view and adopted a ‘drift scanning’ survey technique that eliminated the need for long readout times. At the same time, Rabinowitz (1991) developed the first automated moving object

detection program to identify asteroids and comets in Spacewatch’s drift-scan images that launched the contemporary generation of wide field surveys such as NEAT (Helin et al. 1997), LONEOS (Bowell et al. 1995), LINEAR (Stokes et al. 2000) and CSS (Larson 2007).

These modern wide field asteroid surveys were prompted and subsequently funded by the NASA Spaceguard Program (Harris 2008) with the goal of identifying 90% of Near Earth Objects<sup>1</sup> (NEOs) larger than 1 km diameter before the end of 2008. All the surveys broadly employ similar techniques for asteroid and comet identification. Their wide field cameras have large pixel scales (typically  $\gtrsim 1$  arcsec) and image a field 3-5 times within about an hour. Their moving object detection software identifies ‘sources’ in each image and then spatially correlates the detections between the images to identify and remove stationary objects. All the ‘transient detections’ are then searched for consistency with a single object moving linearly across the sky at a constant rate of motion between the exposures. The constant motion requirement allows the software to achieve per-detection signal-to-noise ( $S/N$ ) levels of  $\sim 1.5$  to  $3\sigma$ . Sets of 3-5 linked detections (a ‘tracklet’) representing candidate real moving objects are reported to the Minor Planet Center (MPC), though some groups review the detections by eye before submission to reduce the false detection rate. Overall, these groups were wildly successful, identifying  $\sim 79\%$  of the  $\geq 1$  km NEOs before 10 June 2008 (Harris 2008). Mainzer et al. (2011) report that the Spaceguard goal of discovering 90% of the  $\geq 1$  km diameter asteroids was actually met some time later but before 2011.

The CCD surveys described above were designed to discover large, extremely hazardous

---

<sup>1</sup>Near Earth Objects are asteroids or comets with perihelion distances of  $\leq 1.3$  AU. Most of these objects are in unstable orbits with dynamical lifetimes of  $< 10$  Myrs (*e.g.* Gladman et al. 2000) and will quickly be ejected from the Solar System or impact the Sun or Jupiter but a small fraction will eventually strike Earth.

NEOs, not to characterize the size-frequency distribution (SFD) of various solar system populations. While the process of searching for the NEOs, they discovered several objects interesting in their own right (*e.g.* Comet Shoemaker-Levy 9, Shoemaker (1995); very fast moving objects, typically very small and nearby asteroids, Rabinowitz et al. (1993); the Centaur object (5445) Pholus; 2008 TC<sub>3</sub>, Jenniskens et al. (2009)); and *post facto* determinations of their surveying efficiency allowed new estimations of the SFD of many small body populations (*e.g.* objects with orbits entirely interior to Earth’s orbit, IEOs, Zavodny et al. (2008); NEOs, Rabinowitz (1993); Main Belt, Jedicke and Metcalfe (1998); Centaurs, Jedicke and Herron (1997); Trans-Neptunian objects, TNOs, Larsen et al. (2001); Distant objects, Larsen et al. (2007)). Despite the success of these programs there is room for improvement in surveying techniques, moving object detection software, and reporting and follow-up methods:

- Survey Technique and/or depth

The surveys in operation in 2003 were not capable of meeting the Spaceguard Goal due to their sky-plane coverage and/or limiting magnitude (Jedicke et al. 2003). These surveys concentrated on the region of sky near opposition because asteroids are generally brightest in that direction but objects on orbits that *will* impact the Earth are under-represented towards opposition. Their sky-plane density increases at relatively small ecliptic latitudes and solar elongations  $\lesssim 90$  deg (*e.g.* Chesley and Spahr 2004; Vereš et al. 2009). However, asteroids in this region of the sky are notoriously difficult to observe because of the limited time that they are above the horizon, the high air mass when they are visible, their large phase angle (reduced illumination of the visible surface) and faintness. Furthermore, the 3-5 repeat visits/night to the same field is wasteful of survey time. More sky could be covered or the same sky could be imaged to greater depth if there were fewer visits to

the same field each night.

- Follow-up

To maximize survey coverage and their discovery rate most of the surveys visit a field on only one night per lunation to obtain a set of 3-5 linked detections. The detections provide the sky plane location and velocity vector for the object rather than an orbit. To identify NEOs, the surveys flag objects with unusual rates of motion (*e.g.* Rabinowitz 1991; Jedicke 1996) as NEO candidates and then reacquire the objects in special follow-up efforts that reduce the time available for discovery of new objects. Alternatively, they report the detections to the MPC who then perform a more sophisticated probabilistic analysis to determine the likelihood that the object may be a NEO. If the object meets their likelihood cutoff, it is posted on their NEO confirmation webpage<sup>2</sup> and hopefully recovered by professional and amateur astronomers around the world. Given that telescope time is a valuable commodity and that the next generation of professional asteroid survey telescopes will discover more and even fainter objects, it is clear that the survey telescopes must provide their own target follow-up and it should be incorporated directly into their survey pattern.

- Moving Object Detection and Orbit Determination Software

With limited follow-up resources and inefficiency in the ability to determine if a candidate asteroid is likely a NEO based on its magnitude and apparent rate of motion (its ‘digest’ score), it would be useful for a survey’s moving object detection system to determine orbits from observations over multiple nights instead of merely reporting sets of detections (tracklets) to the MPC. This allows for improved discovery rates of NEOs that are ‘hidden in plain sight’, indistinguishable from main-belt asteroids by

---

<sup>2</sup><http://www.minorplanetcenter.net/iau/NEO/ToConfirm.html>

their brightness and velocity vectors alone, and therefore scoring too low using the MPC’s NEO digest scoring to warrant follow-up.

- Reporting

The system of reporting sets of detections to the MPC has been very effective and the follow-up response of the international community of amateur and professional observers has been fantastic as amply demonstrated by the case of 2008 TC<sub>3</sub> (Jenniskens et al. 2009). Still, the process of submission by email to the MPC, posting on the NEO confirmation page, downloading and acquisition by observers is unwieldy. Since there is little coordination between observers there is the potential for wasted time with multiple and unnecessary follow-up. A modernized, automated reporting system tuned specifically to the capabilities and interests of each follow-up observatory would be useful to coordinate the follow-up effort.

- Measured System Efficiency

Existing asteroid detection software packages do not monitor their own detection efficiency and accuracy. Instead, analysis of the survey data must be performed *post facto*. It would be convenient if the packages incorporated an intrinsic near real-time measure of both their efficiency and accuracy for the purpose of system monitoring and subsequent data reduction.

Some of the problems itemized above have been addressed by other surveys, in particular the well-characterized main belt program of Gladman et al. (2009) using software developed by Petit et al. (2004). They generate synthetic detections in the same images used to identify their TNO candidates to measure the detection efficiency and accuracy.

The future of wide field moving object processing systems is embodied in software such as the Panoramic Survey Telescope and Rapid Response System (Pan-STARRS;



Kaiser et al. 2002; Kaiser 2004) Moving Object Processing System (MOPS), described in the remainder of this paper. MOPS incorporates state-of-the-art spatial searching, orbit computation and database management into a cohesive package. MOPS resolves many of the issues described above and the system is capable of very high efficiency and accuracy.

## 2. Pan-STARRS and Pan-STARRS1

The University of Hawai‘i’s Pan-STARRS project was formed in 2002 to design and build a next-generation distributed-aperture survey system called Pan-STARRS4 (Kaiser et al. 2002). The Pan-STARRS4 design incorporates four distinct telescopes on a common mount on the summit of Mauna Kea. Shortly after inception, the project began development and construction of a single-telescope prototype system called Pan-STARRS1 (Hodapp et al. 2004; Morgan et al. 2006) on Haleakala, Maui to validate essential components such as optics, camera and software pipelines. As of 2013, the Pan-STARRS project is constructing a second telescope called Pan-STARRS2 essentially identical to Pan-STARRS1, at the same site on Haleakala. The combination of Pan-STARRS1 and Pan-STARRS2 is called PS1+2, and it is expected that the two telescopes will be operated together as part of a single science mission.

The Pan-STARRS1 telescope on Haleakala, Maui, began surveying for asteroids in the spring of 2010. This 1.8 m diameter telescope has a  $\sim 7$  deg<sup>2</sup> field of view and a  $\sim 1.4$  gigapixel orthogonal transfer array (OTA) CCD camera (Tonry et al. 1997, 2004) with 0.26'' pixels. Pan-STARRS1’s large aperture, field of view and  $\lesssim 13$  s between exposures allows imaging of the entire night sky visible from Hawai‘i to  $r \sim 21.2$  in about 5 or 6 nights. In practice, 2 to 8 images of the same field are acquired each night and consequently it takes longer to cover the entire night sky.

The Pan-STARRS1 telescope is operated by the Pan-STARRS1 Science Consortium (PS1SC; Chambers 2006, 2007) with a nominal mission of 3.5 surveying years. The PS1SC survey plan incorporates about a half dozen sub-surveys but only three are suitable for moving object discovery (all the surveys are suitable for moving object *detection* because they all obtain at least one pair of images of each field each night) — the  $3\pi$  all-sky survey, the Medium Deep (MD) survey and the solar system survey.

The Pan-STARRS1 detector system employs six passbands:  $g_{P1}$ ,  $r_{P1}$ ,  $i_{P1}$ ,  $z_{P1}$ ,  $y_{P1}$  and  $w_{P1}$ . Tonry et al. (2012) provide a detailed description of the Pan-STARRS1 photometric system — the first four passbands were designed to have similar characteristics to the SDSS (*e.g.* Karaali et al. 2005),  $y_{P1}$  was designed to take advantage of the good sensitivity of the Pan-STARRS1 camera near  $1\mu\text{m}$  and the  $w_{P1}$  has a wide bandpass with high and low wavelength cutoffs designed to optimize the  $S/N$  for S and C class asteroids. Transformations from each filter to the  $V$  band are provided in table 1 for an object with solar colors and also for an object with an average S+C class spectrum. The difference between the solar and mean asteroid class transformations are significant since the Pan-STARRS1 photometric system currently provides better than 1% photometry (Schlafly et al. 2012) in at least the  $3\pi$  survey’s filters.

The  $3\pi$  survey images the entire sky north of  $-30^\circ$  declination multiple times in three passbands ( $g_{P1}$ ,  $r_{P1}$ ,  $i_{P1}$ ) in a single year. About half the sky within  $\pm 30^\circ$  (two hours) of opposition in R.A. is imaged in the different passbands each lunation. The solar system survey is performed in the wide filter ( $w_{P1}$ ) and most of that time is spent near the ecliptic and near opposition to maximize the NEO discovery rate. A small percentage of solar system survey time is used to image the ‘sweet spots’ for Potentially Hazardous Asteroids<sup>3</sup>

---

<sup>3</sup>PHAs are NEOs with orbits that approach to within 0.05 AU of the Earth’s orbit and have absolute magnitudes  $H < 22$ .

(PHAs) within about  $\pm 10^\circ$  of the ecliptic and as close to the Sun as possible subject to altitude, sky brightness constraints, *etc.* The MD survey obtains 8-exposure sequences at 10 different fixed footprints on the sky, with an integration time of 1920 seconds per sequence. MD sequences are observed using either  $8 \times 240$ -second exposures in a single filter ( $i_{P1}$ ,  $z_{P1}$ ,  $y_{P1}$ ), or back-to-back sequences of  $8 \times 120$ -second exposures in  $g_{P1}$  and  $r_{P1}$ .

Visits to the same footprint within a night are usually separated by about 15 minutes, a ‘transient time interval’ (TTI), suitable for asteroid detection. The Image Processing Pipeline (IPP; Magnier 2006) produces a source list of transient detections, *i.e.* new sources at some position in the image and/or those that change brightness but are otherwise not identifiable as false transients like cosmic rays or other image artifacts. The IPP then publishes the catalogs of transient detections to MOPS which searches for moving objects.

### 3. The Pan-STARRS Moving Object Processing System (MOPS)

#### 3.1. Overview

MOPS software development began in 2003 under management by the Pan-STARRS Project, with a mission to discover hazardous NEOs and other solar system objects while providing real-time characterization of its performance. Initial funds for Pan-STARRS construction and engineering were obtained by the University of Hawai‘i via a grant from the United States Air Force Research Laboratory (AFRL). MOPS was the first and only science client to be funded by the Pan-STARRS Project — systems engineering, testing, performance tuning and creation of the Synthetic Solar System Model (S3M, §3.10) were directly supported by project resources. Additional in-kind software contributions from external collaborators in the areas of orbit determination (Granvik et al. 2009; Milani and Gronchi 2010), spatial searching (Kubica et al. 2007) and algorithm design

(Tyson and Angel 2001) were incorporated via memoranda of understanding (MOUs). In 2008, the NASA Near Earth Objects Observations (NEOO) Program Office began its support of continued MOPS development and Pan-STARRS1 operations.

MOPS is the first integrated detector system that processes data from per-exposure transient detection source lists through orbit determination, precovery and attribution. We sought to create a system that could independently measure our system’s end-to-end throughput and efficiency for the purpose of correcting for observational selection effects (Jedicke et al. 2002). Our philosophy was that it is more important to accurately know the system efficiency than to place all our effort in optimization. Figure 1 provides a high-level view of data flow into, through and from MOPS. Each of the MOPS data processing sub-steps is described in the following subsections.

In the Pan-STARRS system design there is a functional separation between the image processing (IPP) and moving object processing (MOPS). Unlike the object detection algorithm of *e.g.* Petit et al. (2004), the MOPS design mandates no integration with the image data. This was an intentional design decision based on the scale and organization of the Pan-STARRS project. The IPP is responsible for monitoring and reporting its detection efficiency and accuracy as is MOPS. In this way each Pan-STARRS subsystem can be developed and characterized independently.

MOPS data processing consists of assembling groups of transient detections into progressively larger constructions until there are enough detections to produce a high-quality orbit believed to represent a real asteroid — a ‘derived object’. Intra-night (same night) detection groupings are called ‘tracklets’ and inter-night (multi-night) groupings are called ‘tracks’. All tracks created by MOPS are evaluated by an orbit computation module after which a track is either 1) deemed to represent a real asteroid, or 2) rejected and its constituent tracklets returned to the pool of unassociated tracklets. When a derived

object is created MOPS uses the object’s computed (derived) orbit to search for additional detections of the asteroid in MOPS data to further refine the orbit.

MOPS expects its incoming transient detection stream to be organized by exposure, or *field* in MOPS parlance. Each field within MOPS is defined by its metadata *e.g.* (right ascension, declination [RA, dec]) boresight coordinates, exposure date and duration, filter. A MOPS detection by definition occurs in exactly one field and is defined by its position *e.g.* (RA, dec) in the field, observed magnitude, signal-to-noise ( $S/N$ ), and associated uncertainties.

### 3.2. Pipeline Design

The MOPS pipeline operates by using a linear nightly processing model where data are ingested and processed in the order they are observed. Nightly data are ingested from a live transient detection stream and discrete processing stages are executed until all processing is completed for the entire night. Many of the MOPS processing stages build upon data structures created from prior nights.

Out-of-order processing can be handled in a limited number of modes of operation as necessitated by the current Pan-STARRS1 system. Enhancements to the MOPS pipeline to perform full processing on out-of-order data while preserving essential MOPS efficiency computations is still under development. The fundamental difficulty in out-of-order processing lies with the amount of data that needs to be recomputed when new observations are inserted in the middle of the temporal data stream. The existing MOPS design prefers nights to be added incrementally; insertion into the middle of the existing dataset essentially forces all subsequent nights to be reprocessed.

Pipeline resource scheduling and management are handled by the Condor high-

throughput-computing software (Thain et al. 2005). Condor provides effective, flexible management of hardware resources that need to run the MOPS production pipeline simultaneously with test simulations or experimental processing of MOPS data.

The MOPS pipeline is designed to be reliable in the event of cluster resource limitations and hardware failure (*e.g.* power outages, node failures). Working in tandem with Condor’s process management infrastructure, the MOPS pipeline can be restarted easily at the proper point in the pipeline with all data structures intact. As an example, in 2011 the MOPS production MySQL database suffered a complete failure yet the MOPS pipeline was back online within hours after restoring the database from a backup.

The discussion of each element of the MOPS pipeline is deferred to §5 where we follow the processing of detections from beginning to end of the pipeline and quantify the performance of each step using Pan-STARRS1 data.

### 3.3. Hardware

The Pan-STARRS1 MOPS runs on a modest cluster of standard Linux rack-mounted computers. MOPS makes no special demands on hardware so long as the cluster can keep up with incoming data. During early stages of MOPS design we based hardware requirements on estimates for transient detections stored and orbits computed per night of observing for a Pan-STARRS4-like mission, and scaled down the storage for Pan-STARRS1 volumes. The current Pan-STARRS1 processing hardware is capable of keeping up with a Pan-STARRS4-like data stream except for the storage of detections in the database. Table 2 lists the major hardware components employed by the Pan-STARRS1 MOPS production processing cluster, and Fig. 2 shows the functional relationships between the MOPS hardware components.

To ensure against most of the types of disk failures we are likely to encounter, we use a multiple-parity redundant array of independent drives (RAID6) for our database storage, meaning multiple parity bits for every byte stored on disk. This allows up to two drives to fail concurrently and still keep the disk array operational.

Condor’s workflow management automatically detects host-level failures and redistributes jobs appropriately. An entire cluster computation node can fail during a processing step and the MOPS pipeline will adjust seamlessly.

MOPS pipeline administrative functions are handled by a ‘fat’ workstation-class computer that runs the main MOPS pipeline, Condor manager and MOPS web interface (described later). We distribute these functions between two identically configured hosts so that one can fail completely, its responsibilities then assumed by the other node at slightly degraded performance. During Pan-STARRS1 commissioning and operations we have experienced complete database host failures, accidental deletion of a production MOPS database by a MOPS administrator, and numerous compute node failures, without loss of data or significant interruption of MOPS processing.

### 3.4. Database

Table 3 shows the storage required for MOPS database components under Pan-STARRS1 and estimates for Pan-STARRS4. The catalog of high-significance detections and derived data products are stored in an industry-standard relational database to maximize interoperability with external analysis software and provide data mining capability. Data are organized into multiple row-column tables in which rows of one table may be related to rows in another table (see fig. 3). For example, the MOPS FIELDS table contains exposure metadata describing the telescope pointing, exposure time, filter, *etc.*

for a single exposure. Each FIELD record is additionally assigned a unique identifier called FIELD\_ID. A second table called DETECTIONS contains all transient detections ingested by MOPS and, to relate detections to a particular exposure, all detections from the exposure are assigned a FIELD\_ID upon ingest that matches their exposure’s FIELD\_ID . Subsequent derived relations (*e.g.* groupings of detections into an asteroid ‘identification’ and computation of its derived orbit) are similarly maintained and are described in detail later.

A relational database allows MOPS data to be manipulated, analyzed and queried by any external software that supports structured query language (SQL). Requests for both a small amount of data (such as a detection) or a large amount of data (*e.g.* all derived objects with  $q < 1.3$ ) are made through a SQL query and the results are returned in a tabular representation.

The MySQL relational database management system (RDBMS) was selected for MOPS because of its combination of performance and cost but other database vendors such as PostgreSQL and Oracle were considered and evaluated early in MOPS development. Any modern database system would work for MOPS as they all scale to billions of rows and have additional features that promote data integrity and system reliability.

### 3.5. Low Significance Database

MOPS was designed to perform searches for recovery observations using a lower-significance data archive called the ‘low-significance dataset’ (LSD). In normal MOPS processing a nominal confidence level, typically  $5\sigma$ , is used as a baseline for all processing. The Pan-STARRS4 camera and image processing are expected to deliver  $\sim 1500$   $5\sigma$  detections per exposure. Below this confidence level the density of false associations



becomes so great that it overwhelms the data processing. However, the search for recovery or precovery observations of an object with a known orbit may constrain the predicted position and velocity enough to make it possible to identify observations in the LSD.

Due to the much larger number of lower-significance sources in an astronomical image (there are  $1,000\times$  more  $3\sigma$  than  $5\sigma$  detections) LSD detections are *not* stored in the MOPS relational database. Instead, they are stored in flat files on the local or network file system. The LSD archive is designed to be compact and efficiently searchable by exposure epoch, right ascension and declination. During only the attribution and precovery phases of MOPS processing, candidate  $3\sigma$  recovery observations are extracted for analysis from this dataset based on predicted positions, and successful recoveries are then ‘promoted’ into the high-confidence database.

### 3.6. Data Exchange Standard

Significant work related to early MOPS development and simulations led to creation of the Data Exchange Standard (DES) for Solar System Object Detections and Orbits<sup>4</sup>. The DES describes a file format for dissemination of observations and orbits of solar system objects and is used within MOPS and between MOPS and add-on MOPS software developed by A. Milani and the OrbFit Consortium (Milani et al. 2008, 2012). It provides mechanisms for reproducing detection $\Leftrightarrow$ tracklet and tracklet $\Leftrightarrow$ derived object relations that exist in the MOPS database, and allows for specification of statistical uncertainties for observational measures. The DES includes provisions for propagating

---

<sup>4</sup>see Pan-STARRS document PSDC-530-004 by Milani *et al.*, *Data Exchange Standard (2.03) for solar system object detections and orbits: A tool for Input/Output definition and control*.

- orbit covariance and normal matrices,
- detailed per-detection residuals,
- ephemerides for real and synthetic asteroids,
- detailed tracklet metrics beyond the scope of MOPS, and
- radar and spacecraft observations.

### 3.7. Web Interface

Early in MOPS development we realized the utility of visual, web-based interrogation of the MOPS database, leading to the creation of the MOPS *web interface*. The MySQL RDBMS provides software ‘hooks’ into its internal code that allow web-friendly scripting languages to perform queries so that web-based user interfaces and reporting tools can be developed rapidly.

The MOPS database user has ready visual representation of the MOPS processing stream, from a sky map of the nightly survey pattern, detection maps of each observed field indicating both synthetic and real detections, to the orbit distributions of derived objects, to the efficiency and accuracy of each of the processing steps. Pages for a single MOPS derived object show the object’s linking history and the evolution of its orbit at each step. Fig. 4 shows the nightly sky map of an active MOPS database.

### 3.8. Data Export

The primary consumer of MOPS exported data products is the IAU Minor Planet Center (MPC) that maintains the authoritative catalog of observations and orbits for

minor planets, comets and natural satellites. As of early 2013, the MPC prefers email data submission because the Pan-STARRS1 survey is oriented toward reporting single-night tracklets, not multiple-night derived objects.

Under the Pan-STARRS4 processing model where MOPS produces derived objects with secure orbits on a regular basis, MOPS is capable of exporting monthly DES catalogs of detections, tracklets, orbits and identification records for known and unknown derived objects. Pilot submissions to the MPC showed that this export and publication model works as long as the false derived object rate is suitably low (*e.g.*  $< 0.1\%$ ; Spahr, personal communication).

Early Pan-STARRS1 processing revealed a false derived object rate too high for automatic submission to the MPC and an unsatisfactory NEO discovery rate so, to improve the short-term science output and satisfy funding agency requirements, the PS1SC abandoned the derived object processing model in favor of the traditional tracklet reporting method employed by other asteroid surveys. Processing of derived objects will be restored for the final post-survey MOPS processing but the derived object throughput will be small due to the Pan-STARRS1 survey strategy being optimized for single-night NEO discovery.

Detections are distributed to the MPC via email after a human ‘czar’ visually verifies that candidates are real using the MOPS web-based interface. (NEO candidates consume most of the czar’s time because of the high rate of false tracklets at high rates of motion.) In this display, a page lists nightly probable real asteroid tracklets with highlighted NEO candidate tracklets (see Fig. 5). Tracklets that belong to known numbered and multi-opposition objects are identified by a MOPS add-on module called `known_server` (Milani et al. 2012) and automatically submitted to the MPC. A MOPS administrative email account receives MPC confirmation email to verify the MOPS submissions. MOPS maintains its own table of submitted tracklets to the MPC for easy reproduction of

submitted detection details and to prevent multiple submissions of the same tracklets.

### 3.9. Alert System

The MOPS Alert System is a software agent that runs independently of standard MOPS processing and searches for events that require immediate notification or follow-up. The specific type of event is user-configurable using a small piece of Python code written by a MOPS scientist or engineer to query for interesting events. A typical example would be a fast-moving near-earth object (NEO) candidate tracklet that is unlikely to be observed again by the survey telescope and/or needs immediate follow-up so that it is not lost. In this case, the alert system identifies the candidate tracklet by its sky-plane rate of motion and the fact that the tracklet’s positions cannot be attributed to a known asteroid. Additional examples of alerts are tracklets of unknown objects with comet-like motion or extended morphology, or known objects with magnitude anomalies that indicate activity.

The alert system allows alerts to be triggered from either a MOPS derived object or an individual tracklet. The alert payload itself is an extensible markup language (XML) VOEvent (*e.g.* Seaman et al. 2011), a standardized data structure that can be consumed by automatic data-processing agents. The alert deployment infrastructure can be changed easily; the current MOPS implementation uses both a restricted internet email distribution list and a private Twitter feed to PS1 Science Consortium partners.

Alerts are organized using a publish-subscribe paradigm in which multiple alert definitions can be published to various ‘channels’ that may be subscribed to by multiple users. For example, a ‘NEO channel’ might publish alerts for near-earth object alerts ( $q < 1.3$  AU) and potentially hazardous objects (NEOs with  $H < 22.5$  and minimum orbital intersection distance  $< 0.05$  AU). Such a channel could be subscribed to by NEO follow-up

organizations. Alerts currently in use by the PS1SC include unusual lightcurves within a single night and detections of objects from asteroid families of interest (*e.g.* Hildas).

### 3.10. Synthetic Solar System Model

One major MOPS innovation is the incorporation of a synthetic solar system model (S3M; Grav et al. 2011) that allows us to monitor MOPS development and measure its performance in real-time operations as quantified by the metrics defined in §3.1. It is important to introduce realistic detections of solar system objects into the processing system to ensure that it can handle real objects and to measure a realistic detection efficiency. The solar system model has been described in detail by Grav et al. (2011) and we only provide a brief overview here.

The S3M is a comprehensive flux-limited model of the major small body populations in the solar system that consists of objects ranging from those that orbit the Sun entirely interior to the Earth’s orbit to those in the Oort cloud. It even includes interstellar objects passing through the solar system on hyperbolic orbits. The S3M contains a total of over 13 million synthetic objects from 11 distinct small body populations with the only requirement being that they reach  $V \leq 24.5$  during the time period from roughly 2005-2015 (the anticipated operational lifetime of the Pan-STARRS survey). The time period requirement only affects a sub-set of the populations in the distant solar system.

The S3M has proven invaluable for developing and testing MOPS but suffers from one major limitation — it only tests the software system for known types of objects. Since we cannot anticipate the properties of an unknown population we supplemented the S3M with an artificial 575,000-object ‘grid’ population. Grid objects have a random and flat distribution in eccentricity ( $0 \leq e < 1$ ),  $\sin(\text{inclination})$  ( $0^\circ \leq i < 180^\circ$ ) and in the angular

elements ( $0^\circ \leq \Omega, \omega, M < 360^\circ$ ). The semi-major axes of the objects were generated using uniform random distributions over six different ranges as provided in table 4. The ranges and number of objects were selected so that the sky-plane density of objects in each range is roughly equal and to provide denser coverage in the semi-major axis ranges that have large numbers of known objects. The absolute sky-plane density of the grid population is 50 per field, a factor of 20-30 less than the realistic S3M on the ecliptic and much higher than the S3M off the ecliptic.

The absolute magnitudes of the objects in the grid population were generated with uniform distributions in each semi-major axis range but with lower limits that decrease (*i.e.* the objects are made larger) according to the square of the semi-major axis so that the objects are visible from Earth.

A major benefit of testing MOPS with the grid population is that they can appear at the poles where the sky-plane density of real or S3M objects is small. §4.3 discusses the results of simulations with the grid population.

### 3.11. MOPS Efficiency Concepts

During  $\sim 4$  calendar years of MOPS development we continuously benchmarked its performance using 3 metrics for each MOPS subcomponent. The metrics count the correct and incorrect associations of synthetic sources available at each MOPS processing step. The metrics are:

- Efficiency

The fraction of available associations that were correctly identified.

- Accuracy

The fraction of associations that are correct, *e.g.* consisting of detections from the

same synthetic object definition.

- **Quality**

The fraction of correct associations that meet or exceed a pre-defined quality metric.

To provide the detailed accounting required to measure system efficiency and accuracy, data structures for each association created in a MOPS processing phase are decorated with a label describing their disposition after processing. These labels describe the detections incorporated in the resulting data structure:

- **AVAILABLE** - the data structure should have been created in the processing phase and is available to be assigned.
- **CLEAN** - the data structure contains only synthetic detections or tracklets that belong to the same synthetic object, *i.e.* is a ‘correct’ data structure. This label might describe a tracklet that is created from two detections of the same synthetic object, or a derived object consisting of three tracklets that are each **CLEAN** and belong to the same synthetic object.
- **MIXED** - the data structure contains only synthetic objects but the detections or tracklets are from different synthetic objects.
- **BAD** - the data structure contains both synthetic and nonsynthetic detections. For tracklets this is a common and normal occurrence since we expect that synthetic detections will occasionally fall near real detections.
- **UNFOUND** - an expected data structure for a synthetic object was not created. **UNFOUND** data structures are ‘dummy’ structures that represent an operation that *should have* happened. For example, if two sequential fields at the same boresight contain two detections of the same asteroid but a tracklet is not created, a dummy tracklet

containing tracklet metadata is created so that the event can be counted and characterized.

- **NONSYNTHETIC** - the data structure contains ‘real’ detections from actual telescope data. **NONSYNTHETIC** data consists of true detections of asteroids and false detections from image artifacts.

The pipeline must ‘peek’ at the input and output data structures before and after a MOPS processing step to assign synthetic labels but this is the only time that the pipeline knows that a data structure is synthetic — the labels are never examined during any MOPS computation or algorithm. Data structures that are ‘contaminated’ — contain mixtures of real and synthetic detections or different synthetic objects — continue to be propagated through the pipeline. The only exception is for **UNFOUND** objects for which dummy structures are created and decorated with the **UNFOUND** label so that these occurrences can be counted by analysis tools.

MOPS uses the labels to calculate the incremental efficiency after each processing stage. For a derived object, the state at each processing stage is preserved so that a ‘paper trail’ exists for each modification. This allows a complete step-by-step reconstruction of a derived object’s history from its tracklets including the ability to indentify the exact processing step where an object was lost or incorrectly modified by MOPS.

### **3.12. Simulations**

The MOPS pipeline is exercised through the creation and execution of a ‘simulation’. Each simulation begins with a collection of telescope pointings called ‘fields’ and a population of synthetic solar system objects whose positions and magnitudes are computed for every field. Objects that ‘appear’ in fields are converted into detections and stored in



the MOPS database as though they were reported from an actual telescope. Detections can be ‘fuzzed’ astrometrically and photometrically using parameters that model the telescope performance; these include sky background, detector noise, and the point-spread function (PSF). The full fuzzing model incorporates a baseline astrometric uncertainty from the plate solutions added in quadrature with a flux-dependent positional uncertainty. Poisson-distributed (in  $S/N$ ) false detections may be inserted in the fields to simulate noise from a real detector. After the injection of synthetic detections for a night the MOPS pipeline is invoked as though operating on real data.

MOPS simulations are used both to verify correct operation of the pipeline and to interrogate performance of a hypothetical survey. A simple verification test consists of creating a small main belt object (MBO) simulation with several nights of synthetic fields spanning two lunations, executing the pipeline, and verifying that all expected MBOs were ‘discovered’ through creation of a derived object and ‘recovered’ via attribution or recovery where possible. In this fashion all essential elements of the pipeline are exercised and verified after software modifications.

For comprehensive testing, a larger, more realistic synthetic population of objects is inserted into the simulation, the MOPS pipeline is executed, and the output provides a quantitative assessment of the system’s efficiency and accuracy. The pipeline is designed to be essentially 100% efficient at creating tracklets and derived objects for MBOs with the designed Pan-STARRS performance.

When evaluating survey performance we configure MOPS to more precisely mimic the astrometric and photometric characteristics using filter- and field-dependent limiting magnitudes and FWHMs. Given the calculated  $V$ -band apparent magnitude for a synthetic asteroid, we calculate its expected signal-to-noise ( $S/N$ ) using per-field detection efficiency parameters, and then generate a fuzzed magnitude and  $S/N$ . From the fuzzed  $S/N$  and the

field’s FWHM we compute the asteroid’s fuzzed right ascension and declination. If there is variation in sensitivity due to sky brightness or airmass, these effects can be modeled by supplying appropriate values for photometric zeropoint or sky noise in the field’s detection efficiency parameters.

During MOPS development we ran thousands of small- to medium-scale simulations for software unit testing and verification. More importantly, we ran several large simulations with synthetic solar system models containing millions of asteroids spanning several years of synthetic PS1 observations. These simulations were run on our modest PS1 MOPS production cluster and took many weeks or months to simulate the multi-year Pan-STARRS mission. For instance, our `full_S1b` simulation used the full S3M population in a 2 year simulation and required  $\sim 180$  calendar days (see §4.1) while our four year NEO-only simulation (`neo_4yr`) required 88 calendar days (see §4.2). At various times during the pipeline processing the cluster was offline for maintenance or power outages but MOPS is designed to be interrupted and restarted.

The upstream image processing subsystem (*e.g.* the Pan-STARRS IPP) can improve MOPS fidelity by providing a Live Pixel Server (LPS) that reports whether a pixel at or near a specific (RA,dec) in an image falls on ‘live’ camera pixels. This service improves MOPS simulations in two ways: 1) by generating synthetic moving object data with behavior that simulates real observations (*e.g.* to account for the loss of field due to the camera fill factor) and 2) accounting for missing detections when attempting to recover known asteroids that are in the field of view. In a single Pan-STARRS1 exposure there are many reasons an area of the detector can be inactive besides simple chip gaps, such as saturation from a bright object in the field of view, or a cell used for guide star tracking. Thus the LPS tells MOPS what areas of the detector are active for any given exposure. If a LPS is not available from the upstream image processing subsystem, MOPS has provisions

for allowing static specification of a detector mask that defines areas on a detector where detections cannot occur (see Fig. 6). Synthetic detections that land on a dead part of the detector (as determined by the LPS) are marked with a special ‘unfound’ decorator so that they can be accounted for but otherwise omitted from all subsequent processing.

For increased simulation fidelity MOPS can accept a per-field detection efficiency for point sources and trailed detections as a function of  $S/N$  and rate of motion so that MOPS can generate more realistic synthetic photometry.

#### 4. MOPS Verification

During MOPS development we undertook several large-scale simulations to probe the performance limits of the MOPS design and implementation and understand where further attention was needed in software development. These simulations consisted of a complete S3M or large S3M subpopulation, a multi-year set of telescope pointings, and detector performance that simulated a Pan-STARRS4 system. Our motivation was to investigate MOPS performance for the Pan-STARRS4 system as specified in its design requirements, not the reduced, changing performance of the single Pan-STARRS1 prototype telescope undergoing development and commissioning.

##### 4.1. 2-year S3M simulation (full\_S1b)

The MOPS 2-year S3M simulation consists of the full S3M and 100,424 fields spanning 245 distinct nights over nearly two years (29 Dec 2007 through 2009 Oct 22). The simulation took  $\sim 3$  months to execute including various interruptions for cluster downtime and maintenance. It assumes a nominal positional measurement uncertainty of  $0.01''$ , a FWHM of  $0.7''$ , a fill factor of 100%, and a constant limiting magnitude of  $R = 22.7$ ,

representing a single idealized Pan-STARRS1 telescope. Poisson-distributed false detections were added to each field at a density of  $\sim 200/\text{deg}^2$ . The simulated field pointings were generated by the TAO survey scheduler<sup>5</sup> configured to produce a Pan-STARRS-like survey covering  $\sim 3,600 \text{ deg}^2$  near opposition and  $\sim 600 \text{ deg}^2$  near each of the morning and evening sweetspots. Each area is visited three times per lunation, with some nights lost due to simulated poor weather. MOPS achieved an overall 99.99997% tracklet efficiency and 99.26% derived object efficiency. Tables 5 and 6 detail the tracklet and derived object efficiencies per S3M sub-population.

For classes other than NEOs, Jupiter-family comets (JFCs) and long-period comets (LPCs), MOPS has an efficiency better than 99% for converting three or more tracklets to a differentially corrected orbit when observed within a 14 day window. For NEOs our performance is not as good, but as stated elsewhere in this work, we have been more concerned with quantifying MOPS performance for various populations than in optimization. MOPS contains many runtime configuration parameters that allow performance of individual modules to be tuned, often at the cost of greater false results. Pan-STARRS1 operations have led the project to a different mode of NEO discovery than originally envisioned, so we have not focused on improving NEO derived object performance. Similarly for LPCs, we can again improve efficiency by tuning MOPS orbit determination modules to reject fewer parabolic or hyperbolic orbits.

Our differential correction performance (§5.5) is probably overstated because the OrbFit initial orbit determination (IOD) software (Milani et al. 2005; Milani and Gronchi 2010) employed by MOPS can perform its own differential correction after IOD, and we elect to use it in this mode. Therefore orbits handed to the JPL differential correction module are almost always close to a minimum in the solution space where convergence

---

<sup>5</sup>©1999-2006 Paulo Holvorcem; <http://sites.mpc.com.br/holvorcem/tao/readme.html>

will occur. MOPS supports other packages besides OrbFit to perform IOD, and in early evaluation of these packages we saw outstanding performance from the JPL differential corrector.

#### 4.2. 4-year NEO simulation (neo\_4yr)

We ran the `neo_4yr` simulation to calculate upper limits on the NEO detection and discovery rates with a Pan-STARRS1-like system. This system differed from the `full_S1b` simulation by using a  $0.1''$  baseline astrometric uncertainty and by containing almost four years of TAO simulated opposition and sweetspot observations over the expected Pan-STARRS1 mission from March 2009 through January 2013. The simulation only used the 268,896 NEO subset of the S3M. We were not able to simulate the Pan-STARRS1 focal plane fill factor, as the code had not been incorporated into MOPS yet, but we felt it would be reasonable to use a 100% fill factor and scale down our results based on true Pan-STARRS1 detector performance. False detections were not added to this simulation to speed up execution time, but the `full_S1b` results showed that this would not impact our results.

The `neo_4yr` simulation found over 9,405 derived objects of which nearly half had orbital arc lengths greater than 30 days. As with the 2-year `full_S1b` simulation the tracklet efficiency is essentially 100%, with 10 out of 105,439 tracklets lost. MOPS linking performance is similar to `full_S1b` (see table 7) but we find that orbit determination performs less well, at 81.7%, purely due to greater RMS residuals across the orbit from the larger astrometric uncertainty. Again, this acceptance threshold can be relaxed to improve efficiency (fraction of correct linkages surviving orbit determination) at a cost of an increase in false linkages.

### 4.3. Grid Simulations

We have run several grid simulations to ensure that we were not tailoring the efficiency to localized regions in  $(a, e, i)$  phase space. However, we do not inject the grid population into the detection pipeline during normal MOPS operations as this would needlessly increase the tracklet linking combinatorics in an artificial and unrepresentative manner.

To illustrate MOPS operations over the entire phase space we ran the real Pan-STARRS1 survey (*i.e.* actual pointings and cadence) for two consecutive lunations with the grid population and a realistic (0.1") astrometric error model. Figures 7 through 9 show that MOPS is  $\sim 100\%$  efficient for semi-major axes in the range from 0.75 AU TO 5,0000 AU, eccentricities in the range  $[0, 1]$  and all possible inclinations. Fifteen fast-moving objects were rejected (out of 190,973) by the rate limit of 5.0 deg/day in the current Pan-STARRS1 production configuration to reduce false tracklets.

Figures 10 through 12 show that the derived object efficiency is consistently high for all synthetic grid objects on orbits ranging from those with semi-major axes well within the Earth's orbit to beyond 100 AU, over all inclinations with no deterioration in the efficiency for retrograde orbits, and for nearly circular orbits to those with  $e \lesssim 1$ . There is a degradation in the efficiency for  $e \sim 1$  due to the orbit determination failing at the highest eccentricities.

One important feature of the grid population is that it includes objects that can appear near the poles where the sky-plane density of real solar system objects is negligible, *i.e.* it allows us to check that MOPS works correctly even for objects at high declinations as shown in Figs. 13 and 14. While tracklet creation efficiency is nearly 100% for all declinations  $\lesssim 88^\circ$ , within  $2^\circ$  of the pole the grid simulation revealed that slightly conservative tracklet acceptance parameters rejected several fast-moving objects. The derived object efficiency is typically  $\gtrsim 95\%$  for declinations ranging from  $-30^\circ$  to the north celestial pole indicating

that the tracklet linking algorithm works across the entire sky. The drops in efficiency to  $\sim 90\%$  are largely due to an inability to compute an initial orbit (see §5.6) which is in turn usually due to a sparse observation cadence for the track.

## 5. MOPS Validation and Real Data

Processing of data from the current generation of surveys has been addressed by software pipelines already employed by Spacewatch (*e.g.* Rabinowitz 1991; Larsen et al. 2001), the Catalina Sky Survey, LINEAR, *etc.*. We did not want to reproduce their work. MOPS was designed for use with a high-quality transient detection stream delivered by a next-generation Pan-STARRS4 or LSST-class survey system with nearly 100% fill-factor and a relatively modest number of systematic false detections. In many respects, despite the much higher data volumes expected from these telescopes, moving object algorithm design is simpler due to the high quality astrometry and photometry of the input data. MOPS performs less effectively with real Pan-STARRS1 data because it is the *prototype* for the next-generation Pan-STARRS4 survey — not a next-generation survey itself.

That said, the Pan-STARRS1 telescope represents a significant step forward in wide field survey astronomy, and has become a major contributor in NEO detection and discovery and the largest single-telescope source of asteroid observations while satisfying multiple, disparate survey programs. We have adapted MOPS to Pan-STARRS1 to maximize asteroid detection and NEO discovery from the Pan-STARRS1 data stream through the creation of tools to reject false detections and tracklets and allow for human review of data before they are submitted to the Minor Planet Center. Additionally, due to a realized survey cadence that is inefficient at producing enough repeat observations to compute reliable orbits, we have de-emphasized MOPS’s derived object functionality in normal Pan-STARRS1 processing. In practice, the MOPS pipeline is executed through the tracklet-creation stage,

with some “add-on” tools that are described below. MOPS is still used to its full capability as a simulation and research tool.

In this section we describe in detail all the Pan-STARRS1 MOPS processing steps and quantify its performance on the transients provided by the prototype telescope.

### 5.1. Pan-STARRS1 Surveying

The Pan-STARRS1 ‘effective’ camera fill factor ( $f$ ) as measured by MOPS is  $\sim 75\%$ . The loss of image plane coverage results from gaps between the OTAs, dead cells and gaps on the CCDs themselves, problematic pixels (*e.g.* anomalous dark current or non-linearity), and the allocation of sub-sections on the OTAs (known as cells) to high speed acquisition of bright guide stars. The original MOPS design assumed  $f \sim 100\%$  (Pan-STARRS4) and three 2-detection tracklets/lunation for new object discovery so that with  $f < 100\%$  the maximum achievable system efficiency ( $\epsilon_{max}$ ) for moving objects must be somewhere in the range of  $f^6 \leq \epsilon_{max} \leq f^1$ , depending on the object’s rate of motion, the distribution of ‘dead’ image plane pixels/area and the telescope pointing repeatability. This implies that the maximum Pan-STARRS1 MOPS end-to-end derived object efficiency for objects in the field of view must lie in the range 26-75% even for objects that would be imaged at high  $S/N$ .

In part to compensate for the fill-factor, in October 2010 the Pan-STARRS1 survey was modified to obtain a four-exposure ‘quad’ in a manner similar to other NEO surveys instead of a single pair of exposures. The 4 images of a quad are typically acquired at the same boresight and rotator angle with a transient time interval (TTI) of about 15 minutes between sequential detections. Thus, a tracklet containing four detections would have a typical arc length of about 45 minutes. We then search for tracklets with three or four



detections in the quad. The false tracklet rate decreases as the number of detections in the tracklet increases but even with 4 detections per tracklet there are still false tracklets. To cope with the false tracklet rate we implemented a NEO ‘czaring’ procedure and an associated infrastructure for extracting ‘postage stamp’  $100 \times 100$  pixel images centered on every detection incorporated into a tracklet. A human observer, the ‘czar’, vets every tracklet before submission to the MPC.

The tracklet processing for pair observations by other Pan-STARRS1 surveys is specifically directed towards NEO detection and is divided into two rate of motion regimes — slow and fast, corresponding to 0.3 to 0.7 deg/day and 1.2 to 5 deg/day respectively. *i.e.* Tracklets containing just two detections are not detected if they have rates of motion between 0.7 and 1.2 deg/day. The reason for the two-regime processing is that the confusion limit from false detections becomes unmanageable around 0.7 deg/day, but beyond  $\sim 1.2$  deg/day we can use trailing information to reduce the false tracklet count. The slow regime’s lower limit corresponds roughly to a rate of motion that easily distinguishes between NEOs and main belt asteroid motions at opposition. The upper limit in the slow regime is set empirically at the rate at which the confusion limit becomes too high for the czar. The gap between 0.7 deg/day and 1.2 deg/day leaves a ‘donut hole’ in the velocity space where pairwise tracklets will not be found. Recent improvements in our ability to screen false detections will allow this hole to be removed when Pan-STARRS1 is observing away from the Galactic Plane.

In the fast pairwise tracklet regime MOPS makes use of morphological information (*e.g.* moments) provided by the IPP as a proxy for trailing information. Quality cuts require similar morphology between the two detections and that the position angles (PA) calculated from the detection moments be aligned with the PA of the tracklet.

## 5.2. Detections

The false detection rate delivered by the Pan-STARRS1 IPP to MOPS is shown in Fig. 15. The rate is dominated by systematic image artifacts rather than statistical noise. At high galactic latitudes the transient detection rate is about the expected value from statistical fluctuations in the background but the rate increases dramatically as the field center approaches the galactic plane where the false detection rate is  $10 - 50\times$  higher than expected. The increase in false detections with proximity to the galactic plane is due to image subtraction issues in regions with high stellar sky plane density and residual charge in the CCDs from bright stars. The transient rate in the  $w_{P1}$  filter does not have data for galactic latitudes  $\lesssim 30$  deg because this filter was solely used for solar system surveying and detection of moving objects. The solar system team does not survey into the galactic plane because we learned early-on that the false detection and tracklet rates are too high to efficiently detect solar system objects.

Overall, the rate of transient detections at  $\geq 5\sigma$  is  $\sim 8200/\text{deg}^2$  — orders of magnitude higher than expected with Poisson statistics and with far more systematic structure, *e.g.* from internal reflections and other artifacts. This structure is especially problematic because, unlike Poisson-distributed false sources that are evenly distributed across the detector, systematic false sources tend to be clumped spatially and form many false tracklets that can clog and contaminate subsequent data processing. A large number of reported false detections for which the  $S/N$  is much lower than expected at a given magnitude could easily be removed with a field-dependent cut on  $S/N$  vs. magnitude (see Fig. 16).

Figure 17 shows a representative sample of the types of false detections provided to MOPS by the IPP. Accurate machine classification of these artifacts using methods such as those described by (Donalek et al. 2008) can greatly reduce contamination and is under exploration by the PS1SC. We use imaginative monikers like ‘arrowheads’, ‘chocolate chip

cookies’, ‘feathers’, ‘frisbees’, ‘pianos’ and ‘UFOs’ to classify them when iterating with the IPP on improving the detection stream. Many of the false detections are easily explained as internal reflections, ghosts, or other well-understood image artifacts but some are as yet unexplained. MOPS screens false detections using their morphological parameters but many survive the cuts into tracklet formation because they must be conservative so that diffuse comet detections are not removed.

Finally, when the density of false detections spikes to rates that are difficult to manage, *e.g.* near a very bright star, we invoke a last-ditch spatial density filter to reduce the local sky-plane density to no more than 10,000 detections/deg<sup>2</sup> in a circle of 0.01° radius. The filter eliminates false detections by discarding those with the highest PSF-weighted masked fraction until the detection density is manageable.

Even real detections are often not well formed PSFs as illustrated in Fig. 18. Trailed detections often intersect with cell and chip gaps (a), PSF-like detections of slower moving objects have overlapping PSFs (2012 PF<sub>12</sub>), or sit on the boundary of a masked region (*e.g.* e). Whenever a detection is poorly formed it creates difficulties in astrometry and photometry and therefore in linking the detections into tracklets and tracks.

Despite these problems Pan-STARRS1 astrometry and photometry reported to the MPC for slow moving objects is currently excellent by contemporary standards. The average RMS astrometric uncertainty is about 0.13" (Milani et al. 2012). The intrinsic photometric uncertainty in the calibrated<sup>6</sup> Pan-STARRS1 data is < 10 mmag in the  $g_{P1}$ ,  $r_{P1}$ , and  $i_{P1}$  filters and  $\sim 10$  mmag in the  $z_{P1}$  and  $y_{P1}$  filters (Schlafly et al. 2012). The asteroid photometry is not yet as good as in the 5 primary Pan-STARRS1 filters because 1) much of the data is in the still to be fully calibrated  $w_{P1}$  filter and 2) the detections

---

<sup>6</sup>Pan-STARRS1 began reporting calibrated magnitudes in May 2012.

are often trailed enough to cause problems with the photometric fit. We expect to solve these problems soon and begin reporting  $w_{P1}$  band photometry for moving objects with a calibration accuracy of a few tens of mmag.

### 5.3. Tracklets

Kubica et al. (2007) provide detailed information on our algorithms and their performance for linking detections of moving objects on a single night into ‘tracklets’ or linking tracklets between nights into ‘tracks’. Their techniques rely on the use of ‘kd-tree’ structures to provide fast and scalable performance.

Their Table 1 shows that the algorithms yield nearly 100% tracklet creation efficiency for the S3M in the presence of the expected but random false detection rate of  $250 \text{ deg}^{-2}$ . About 10-15% of the generated tracklets are MIXED or BAD but this tracklet accuracy is perfectly acceptable because false tracklets should not link together across nights to form a set of detections with a good orbit. The mixed tracklets cause no loss of objects because the tracklet creation is non-exclusive *i.e.* the same detection can appear in the correct CLEAN tracklet and in multiple other tracklets. Kubica et al. (2007) note that the technique still worked with high efficiency even without using the detections’ orientations and lengths but at the expense of a much higher false tracklet rate. Furthermore, they showed that the system maintains its integrity even at  $> 10\times$  higher random false detection rates.

The algorithm for linking tracklets between nights uses a kd-tree to quickly identify candidate tracks. Each track is then fit to a quadratic in RA and Dec with respect to time to eliminate tracks based on their fit residuals. The number of candidate tracks increases exponentially with the number of detections as shown in Table 3 in Kubica et al. (2007) — while 98.4% of the correct tracks are properly identified only 0.3% of the tracks that pass

all the cuts are real. The false tracks are eliminated in the next step through initial orbit determination (IOD) described in the following sub-section.

As discussed in the previous section, tracklet formation must take place in the presence of false detections due to statistical fluctuations on the sky background but also the usually much more numerous and problematic systematic false detections. We note that Kubica et al. (2007) performed their tests using 2-detection tracklets and with assumptions on the astrometric and photometric performance expected for the cosmetically clean images of an idealized Pan-STARRS4 survey. Their simulations are thus not directly applicable to the real Pan-STARRS1 system that includes more noise and degraded astrometry. The Pan-STARRS1 false detection rate is  $10 - 50\times$  greater than expected at  $\geq 5\sigma$  and almost all of them are systematic. They pose problems for MOPS in that the detections “line up” well enough to pass the tracklet formation cuts and the tracklets represent objects with asteroid-like rates of motion. The high false tracklet rate significantly slows down derived object processing because of the resulting tremendous false track rate.

The realized tracklet creation efficiency and accuracy was measured with synthetic detections injected into the real Pan-STARRS1 data. In this data stream typically 4 images are acquired at the same boresight with roughly a TTI separating each image in the sequence. We form tracklets of 2, 3, or 4 detections with some limits on the effective rate of motion depending on the number of detections in the tracklet. Table 8 shows that the tracklet creation efficiency is 99.98% — the algorithm correctly identifies almost every possible set of detections in a tracklet even in the presence of real detections and noise.

The algorithm returns additional MIXED and BAD tracklets though at a small fraction of the CLEAN rate (see §3.1 and §3.11 for definitions). Tracklets are also identified for the non-synthetic detections *i.e.* detections of real objects or false detections. For the purpose of the efficiency and accuracy calculation both types of non-synthetic detections are ‘noise’

as viewed from the perspective of the synthetic solar system objects. Thus, non-synthetic tracklets may be sets of detections of real solar system objects — but the numbers in Table 8 indicate that there is a problem. There are roughly  $7\times$  more non-synthetic detections than synthetic but, if our simulation and synthetic population are an accurate representation of reality, and all the non-synthetic detections are real, the two values should be roughly the same.

Tracklets can only be formed from detections in images acquired within a reasonably short time frame with sequential detections of the same object separated by about a TTI. Linking detections into tracklets across longer time intervals creates a combinatoric explosion that can not be addressed by the current linking algorithms. On the other hand, it often happens that multiple tracklets for the same object are created on the same night separated by time intervals large compared to a TTI. The most common cause is overlap between adjacent fields acquired at times separated  $\gg$ TTI. Even more problematic are ‘deep-drilling’ situations where  $\gg 4$  images are acquired at the same boresight in rapid succession. In this situation a real object moving between the images is not necessarily detected in every image due to *e.g.* chip and cell gaps, passing over a star, masking, photometric fluctuations, *etc.*, and detections from the same object may appear in different tracklets. Furthermore, the detections within the tracklets may overlap in time due to astrometric fluctuations. (*e.g.* detections from images 1, 3 and 6 appear in tracklet A and detections from images 2, 5, and 8 appear in tracklet B with no detections in images 4 and 7.) Thus, when there are  $> 4$  exposures in a sequence at the same boresight we post-process the tracklet list with `collapseTracklets`.

`collapseTracklets` merges co-linear tracklets within a single night or data set using a method similar to a Hough transform. The approximate sky plane location of each tracklet is determined at the mid-time of all tracklets in the set assuming that their motion is

linear in RA and Dec during the time frame ( $\dot{\alpha}$  and  $\dot{\delta}$  respectively). Co-linear tracklets corresponding to the same object should have similar positions and motion vectors making them straightforward to identify as ‘clumps’ in  $(\alpha, \delta, \dot{\alpha}, \dot{\delta})$ -space using a series of range searches implemented with a 4-dimensional kd-tree. Given candidate groupings of tracklets in the transform space, `collapseTracklets` attempts to merge them using straightforward RMS residual acceptance criteria, where there is a basic tradeoff between creating false merges vs. allowing too many duplicates. The cost of duplicate tracklets in the deep-drilling sequences is that if there are duplicate tracklets for the same object, a potential derived object will rightly use the distinct tracklets to create two distinct derived objects for the same object, and derived object discordance rejection (see §5.5) will disallow the derived objects on the grounds that multiple tracklets for an object cannot exist in the same set of fields.

We adopted `collapseTracklets` essentially unmodified upon delivery from the development team at LSST, and beyond simple tests that verify basic capability, we have not attempted to maximize its efficiency with Pan-STARRS1 deep-drilling cadences or data quality. Informal evaluations against the Pan-STARRS1 8-exposure Medium Deep (MD) sequences show a duplicate ratio of  $\sim 25\%$  with essentially zero lost tracklets.

In the time span from February 2011 through May 2012 MOPS created  $1,513 \times 10^3$  tracklets of which  $534 \times 10^3$  were real (35%) and  $345 \times 10^3$  were automatically attributed to numbered or multi-opposition objects (see §5.9). The situation is much worse for tracklets containing just 2 detections:  $11,691 \times 10^3$  created with just  $780 \times 10^3$  attributed (6.7%). Assuming that the attributed:real ratio is the same as for the 3- and 4-detection tracklets it implies that only  $\sim 10\%$  of 2 detection tracklets are real.

In theory, the Pan-STARRS1+MOPS system is capable of detecting the highest proper motion stars within a single lunation. Consider the unusual case of Barnard’s star with

an annual proper motion<sup>7</sup> of  $\sim 10.3''/\text{year}$  or about  $0.0282''/\text{day}$ . Pan-STARRS1’s average RMS astrometric uncertainty is about  $0.13''$  (Milani et al. 2012) so that Barnard’s star shows noticeable astrometric motion in about 5 days. Barnard’s star would be provided as a transient detection to MOPS if the Pan-STARRS1 IPP created difference images using a static sky created from earlier images (Magnier et al. 2008). On each night MOPS would create a ‘stationary’ transient and if the survey provided more detections 5 and 10 days later MOPS would link the tracklets together. Thus, even in normal operations it is theoretically possible that MOPS could provide detections of high proper motion stars light years from the Sun. It takes little imagination to realize that MOPS could process ‘stationary’ tracklets identified in three successive *months* to discover proper motion stars to even larger distances. The false detection rates for image differencing using a static sky should be no worse than pairwise image differences at the same  $S/N$ .

#### 5.4. Tracks

Tracklets are linked into ‘tracks’ across previous nights over a time window of typically 7-14 days using another kd-tree implementation called `linkTracklets` (Kubica et al. (2007)). The MOPS runtime configuration specifies how many days prior to the current night to search and how many tracklets are required to form a linkage. The tracklets search locates combinations of tracklets that collectively fit quadratic sky-plane motion to within some configured error. Of course actual asteroid motions are not truly quadratic, but within the time interval of track creation this approximation holds for most objects.

Column 4 in table 9 shows that the tracklet linking efficiency is  $\sim 80\%$  for most classes of solar system objects ranging from the inner solar system to beyond Neptune. The

---

<sup>7</sup>[http://simbad.u-strasbg.fr/simbad/sim-id?Ident=V\\*+V2500+0ph](http://simbad.u-strasbg.fr/simbad/sim-id?Ident=V*+V2500+0ph)



linking efficiency is reduced from our grid simulations for several reasons: a) linkages are contaminated with false tracklets and fail orbit determination; b) Medium Deep sequences generate multiple tracklets for the same object, causing rejections in the discordance checks (see 5.5); and c) we simply have not yet tuned `linkTracklets`' operational parameters to Pan-STARRS1's current survey mode and astrometric performance. Early MOPS tests with synthetic and real data obtained from Spacewatch (*e.g.* Larsen et al. 2001) showed that the derived object efficiency can be increased to nearly 100% with a suitable survey strategy, false detection rate, and set of `linkTracklets` configuration parameters

Table 9 does not show `linkTracklets`'s accuracy but it is similar to the  $\ll 1\%$  accuracy reported by Kubica et al. (2007). *i.e.*  $\gtrsim 99\%$  of all the tracks are *not* real. However, very few of the tracks survive the subsequent motion, acceleration, astrometric and photometric residual cuts, *etc.* Those that do pass all the cuts are subject to initial and differential orbit determination to eliminate essentially all the bad tracks as described in the following two subsections.

### 5.5. Orbit Determination

MOPS identifies tracks that represent a real or synthetic asteroid through 'orbit determination'. A six-parameter orbit is calculated for each track and only those that do not exceed a RMS residual requirement are accepted and passed on to the next processing phase. Orbit determination is a two-stage process within MOPS beginning with initial orbit determination (IOD) and followed by a least-squares differentially corrected orbit determination. Tracks that do not satisfy the residual requirement are discarded and their tracklets made available for use in other linkages.

Occasionally there may be cases where a tracklet is included in multiple distinct

linkages whose fitted orbits produce RMS residuals that meet MOPS acceptance thresholds. When this occurs the tracklet cannot logically be included in both derived objects, so MOPS includes code ‘discordance identification’ software that identifies this situation and either

- chooses one linkage as ‘correct’ if its RMS residual is significantly smaller than all others, or
- rejects all linkages as bad since no correct linkage can be determined.

Similarly, two distinct tracklets may share a common detection and be included in otherwise separate linkages with acceptable RMS residuals. In this case it is logically impossible for the detection to belong to two different objects, so the discordance identification routines select one linkage as described above or rejects them all if none stands out as correct. Tracklets in rejected linkages can be recovered later in processing through precovery (see §5.10).

## 5.6. Initial Orbit Determination (IOD)

Orbit determination using a small number of observations over a short time interval has been studied for centuries, since Kepler first described the laws of planetary motion. Many techniques have been devised, each with its own advantages, and modern computers allow many different methods to be evaluated for a set of input detections.

For MOPS’s purposes, IOD is a module that produces six-parameter orbits given a set of detections. We implemented the ‘OrbFit’ package developed by the OrbFit Consortium (Milani and Gronchi 2010). Our selection criteria for an orbit determination package were 1) efficiency at producing an orbit given a ‘true’ linkage; 2) orbit accuracy for observations

using Pan-STARRS cadences and astrometric uncertainties; 3) speed of computation; and 4) availability and support. We tested the orbit determination software against millions of synthetic tracks to measure performance. As with other MOPS software, while we wanted high efficiency and accuracy in our orbit determination software, it was equally important to precisely measure the orbit determination efficiency.

Table 9 shows that the IOD efficiency is essentially 100% for all classes of solar system objects. *i.e.* OrbFit successfully provides an orbit when provided a correctly linked set of tracklets (a track).

### 5.7. Differential Correction

MOPS attempts to improve the IOD by navigating the parameter space of orbit solutions to minimize the least-square RMS residual of the fitted detections. As with initial orbit determination, differential correction is a long-studied problem, spanning many decades of research, made routine by today’s computer hardware. Modern differential correction techniques use precise models for the motion of the Earth and other large solar system bodies and are able to predict positions on the sky to within hundredths of an arcsecond many years into the future given enough input observations.

Through a memorandum of understanding (MOU) with the Jet Propulsion Laboratory (JPL) Pan-STARRS obtained permission to use a subset of JPL’s Solar System Dynamics (SSD) software to compute asteroid ephemerides and differentially corrected orbits. SSD is a workhorse of solar system analysis, used for guiding spacecraft missions to their asteroid and comet destinations and for assessing impact probabilities for high profile NEOs.

Table 9 shows that the differential correction efficiency for objects that have passed IOD is essentially 100% for all classes of solar system objects.

Despite the overall effectiveness of the OrbFit IOD+JPL differential corrector combination, certain geometric configurations can lead to convergence to an incorrect orbit — the motion of objects in the small-solar-elongation sweetspots leads to dual solutions for orbits computed with short arcs. For short windows around the orbit computation, typically up to 30 days, the ephemeris uncertainty using the ‘wrong’ orbit is small enough that an attribution or precovery tracklet can still be found. With the additional arc length from the attribution or precovery the new orbit will collapse to a single solution.

### 5.8. Derived Objects

The tracklets and orbital parameters of tracks that survive the RMS residual cuts for orbit determination are stored in the MOPS database as a ‘derived object’. A derived object represents a moving object ‘discovered’ by MOPS; in other words, the detections are believed to belong to the same body with an orbit that allows the body’s motion to be predicted well enough to recover the body in an adjacent lunation to the discovery lunation.

The derived object efficiency and accuracy is provided in table 9. The realized efficiency for the Pan-STARRS1 survey is currently in the 70-90% range for most classes of solar system objects. Due to the high false detection rates the survey has concentrated on identifying candidate NEO tracklets by their anomalous rates of motion (*e.g.* Rabinowitz 1991; Jedicke 1996) and has temporarily abandoned the idea of creating derived objects. Despite a survey pattern, cadence and un-optimized MOPS configuration that are not particularly well-suited to creating derived objects, the system still achieves 70-90% efficiency for objects that appear in multiple tracklets within a lunation.

### 5.9. Attribution of known objects

MOPS was designed to operate agnostically on all tracklets regardless of whether they correspond to known or unknown objects. *i.e.* no *a priori* information about known objects is used when creating MOPS tracklets, tracks or derived objects. The motivation was to create a final set of ‘derived objects’ from Pan-STARRS1-only data with good controls on observational selection effects.

On the other hand, for the purpose of extracting more science from the data, and as an alternate means of measuring the system’s detection efficiency and accuracy, we also attribute tracklets to known numbered and multi-opposition asteroids using Milani et al. (2012)’s `known_server` module. They show that it has essentially 100% efficiency and 100% accuracy using Pan-STARRS1 data for those classes of objects and subsection §5.13 discusses the realized Pan-STARRS1+MOPS detection efficiency characteristics using the known objects.

As of October 2012 we have reported detections for approximately 240,000 numbered and 84,000 multi-opposition objects identified by `known_server` to the MPC. These detections represent about 73% of the total 3.4 million detections, the remainder being mostly previously unknown asteroids. The fraction of known objects decreases with increasing  $V$ -magnitude such that 50% of the reported objects are unknown for  $V > 21.6$  (see Fig. 19).

### 5.10. Precovery & Attribution (‘PANDA’) of derived objects

In keeping with the principle of MOPS agnosticism with respect to previously known objects we implemented the capability within MOPS to ‘attribute’ new tracklets each night to MOPS’s derived objects. Recall that the time window for creating a MOPS derived

object is typically 7-14 days, but we want to associate individual tracklets from new data with existing derived objects if possible (attribution), and search the MOPS database for individual tracklets observed previously that did not form a derived object because not enough tracklets were observed at the time (precovery). Early Pan-STARRS work showed that with sufficiently high-quality astrometry, an orbit with arc length of typically 10-14 days would have a prediction uncertainty small enough to locate the object in an adjacent lunation. Then, after a successful precovery or attribution extends the arc to beyond 30 days, the orbit is secure.

The PANDA algorithm is a simplified version of that described by Milani et al. (2012) — in essence we integrate every derived object’s motion to the time of observation of each image and compare the predicted location and velocity to all nearby tracklets to see if there is a match. If there is a match we attempt a differential orbit computation and if the resultant fit and residuals are within acceptable bounds we attribute the tracklet to the derived object. In practice, we pre-determine the locations and velocities of all derived objects at the beginning, middle and end of the night and then use `fieldProximity` (Kubica et al. 2005) which interpolates their locations and velocities to each image time and uses a kd-tree implementation to make candidate associations between derived objects and tracklets.

Table 10 shows that the attribution efficiency is  $\sim 93\%$  but it is important to keep two points in mind: 1) this is the cumulative efficiency for *all* possible attributions on that night and 2) the statistics are dominated by the main belt asteroids. In regard to the first point, our efficiency determination software knows when a new synthetic tracklet is detected for an existing synthetic derived object but it does not account for the accuracy of the derived orbit’s ephemerides at the time of observation *e.g.* the derived object’s arc-length. It may be that the available attribution was for a derived object detected on each of the last 3

nights or it may be a derived object whose last observation was 3 years beforehand. Thus, we expect that attribution efficiency will decrease as a function of time. Even though the results in table 10 are dominated by the main belt the attribution efficiency mostly increases with the semi-major axis of the object — it is relatively easy to attribute distant, slow moving objects because their sky plane density is low and their motion is mostly along a great circle, and it is difficult to attribute nearby objects for the opposite reasons.

The mixed and bad attributions in table 10 are of particular concern (see §3.11 for definitions of the terms). In these types of attributions *unassociated* detections are added to the derived object. *i.e.* the derived object is being contaminated by noise or detections of other objects. Since the synthetic MOPS objects are intended to mimic the behavior of the real objects we assume that the real objects suffer the same ‘contamination’ levels (from real and synthetic detections and from false detections). Some level of contamination is always unavoidable but it will degrade the quality of the derived orbits so that future attributions are less likely to be real.

There are several ways to mitigate the contamination including 1) tighter controls on the residuals of candidate detections added to derived objects or 2) *post-facto* ‘scrubbing’ of all derived orbits to identify outlying detections associated with derived objects. We never implemented these techniques and have essentially abandoned improvement of the attribution algorithm because it was designed for a survey pattern that would provide  $\geq 3$  tracklets for most observed asteroids in each lunation.

The complement to attribution is ‘precovery’ in which historical unattributed tracklets are linked to new derived objects. Our precovery algorithm is essentially identical to attribution but applied backwards in time. The only enhancement is that when a successful precovery enhances the derived orbital element accuracy with a consequent reduction in the ephemeris errors we iterate on the precovery attempts until all possible precoverable

tracklets are associated with the new derived object.<sup>8</sup> We also allow for the precovery of tracklets intermediate in time between existing tracklets in the derived object.

When the observed arc length of a derived object exceeds a configurable time span such that the prediction uncertainty over the entire survey is below some threshold, the object has reached a stage where the orbit solution is stable, all possible detections have already been associated with the object, and it no longer needs to be precovered. This optimization reduces the processing time required for precovery (see Fig. 20) because over a long enough survey many objects will be ‘retired’ out of precovery when their orbits become sufficiently accurate. For synthetic objects, MOPS records all successful and failed precoveries so the pipeline can produce statistics on objects that have reached orbit stability but still have recoverable tracklets (see table 11).

Fig. 21 illustrates the sequence of events within MOPS for a hypothetical asteroid that is observed over three successive lunations. For synthetic objects, the ‘paper trail’ allows us to interrogate derived object performance and understand how and what kinds of objects get lost in the system. For each derived object ‘event’ (derivation, attribution, or precovery), the object’s orbit is modified (hopefully improved) and recorded, allowing easy inspection of the orbit history for the derived object within MOPS.

### 5.11. Orbit Identification

When a new derived object ( $A'$ ) is created it is automatically checked for possible precoveries as described above. If the arc length is still short even after precovery it is possible that much earlier detections of the object  $A'$  appear in the database that can

---

<sup>8</sup>The precovery algorithm is invoked any time any orbit changes. *i.e.* the attribution of a new tracklet to an existing derived objects also triggers the precovery algorithm.



not be precovered because the ephemeris uncertainty becomes too large when the current derived orbit is integrated backwards in time. On the other hand, those much earlier detections may also have been incorporated into a derived object ( $A$ ) that similarly can not be attributed to the current detections because integrating derived object  $A$  forward in time generates too large an ephemeris uncertainty. Thus, the same object may exist in two separate derived orbits that are unlinkable by our precovery and attribution techniques.

Rigorous techniques exist for ‘orbit identification’ — associating short arcs of detections within an apparition to the same object observed with a short arc in another apparition (*e.g.* Granvik and Muinonen 2008; Milani et al. 2005) — but given the high astrometric quality we could assume for Pan-STARRS4, we adopted a simplified strategy that searches for neighboring orbits in orbit parameter space.

If each of the two derived orbits are themselves reasonably accurate and precise then it is possible to identify the two derived objects as being identical simply by checking that the derived orbit elements are similar. Given that we expected to find  $> 10^7$  objects with Pan-STARRS and thousands of new derived objects each night we implemented the search for similar derived orbits in a kd-tree (`orbitProximity`). For any new derived object  $A'$  `orbitProximity` identifies a set of candidate derived orbits ( $X = \{A, B, C, D\}$ ) for which all six orbit elements match  $A'$  to within the tolerances shown in table 12. Then we attempt a differential correction (§5.7) to an orbit including all detections from pairwise combinations of  $A'$  with each of the candidate orbits. *e.g.*  $\{A, A'\}$ ,  $\{B, A'\}$ . If the differentially corrected orbit meets our *RMS* residual requirements then the two derived objects are merged into one derived object (*e.g.*  $A$  and  $A'$ ).

Our MOPS simulations for a Pan-STARRS4 system showed that the orbit identification efficiency and accuracy were close to 100% using the tolerances in table 12. The realized orbit identification efficiency for Pan-STARRS1 is  $\sim 26\%$  as show in table 13. The

reduced efficiency is because the Pan-STARRS1 cadence and astrometry yields orbits with uncertainties larger than our configured orbit identification tolerances.

### 5.12. Data Rates & MOPS Timing

Figure 20 shows execution times for various MOPS processing stages over one year of a 2-year MOPS simulation with the S3M. Processing times for per-night stages within the pipeline (generation of synthetics and tracklets) are generally constant, while stages that operate on the simulation’s internal catalog of derived objects grows linearly or worse, depending on gross algorithmic considerations. Naively, the precovery stage exhibits quadratic growth, as the number of derived objects seen by MOPS and the number of precovery images to search both grow linearly as a function of simulation time, but optimizations in the precovery algorithm that limit the search windows reduces this growth below quadratic ( $\sim O(n \cdot \log n)$ ).

The bimodality of timing results in Fig. 20 is due to the survey containing nights with either sweetspots (168 exposures) or opposition regions (660 exposures) or both. The slow growth of the synthetic generation stage is due to the increased integration time required to produce a position for an asteroid at the observation epoch from the survey start date. Recent MOPS versions eliminate this overhead by periodically propagating the epoch of S3M orbits to the current end-of-survey. Inter-night linking and orbit determination computation time grow slowly as the size of the MOPS database increases.

### 5.13. Detection efficiency

Figure 22 illustrates the realized tracklet detection efficiency of the combined Pan-STARRS1+MOPS systems as measured using asteroids attributed (or not)

by `known_server` (see §5.9). The data in each filter were fit to the function  $\epsilon = \epsilon_0 \left[ 1 + \exp \left( [V - L]/w \right) \right]^{-1}$  where  $\epsilon_0$  represents the maximum efficiency for bright but unsaturated detections,  $V$  and  $L$  are the apparent and limiting  $V$ -band magnitudes respectively, and  $w$  is the ‘width’ of the transition from maximum to zero efficiency. The limiting magnitude  $L$  is the magnitude at which the efficiency is 50% of the maximum value. The magnitudes in all bands were converted to  $V$  using a mean C+S class asteroid type as shown in table 1. The function is a good representation of the efficiency near the limiting magnitudes and the scatter at bright values is simply due to low statistics.

The maximum efficiency in all 4 filters in Fig. 22 is  $\sim 78\%$  which is almost entirely driven by the effective Pan-STARRS1 camera fill factor of  $\sim 80\%$ . This implies that when a asteroid is imaged on a live and unmasked camera pixel it is detected with  $\sim 97\%$  efficiency. The limiting magnitudes in  $g_{P1}$ ,  $r_{P1}$ , and  $i_{P1}$  are roughly equal at  $V \sim 20.5$  and any difference between the bands is due to unbalanced exposure times. The wide-band filter  $w_{P1}$  goes  $\sim 1$   $V$ -mag deeper through a combination of the 45 second exposure time and its  $\sim 3\times$  higher bandwidth.

Figures 23 and 24 show that Pan-STARRS1+MOPS performance was roughly constant over the first year of operations. The dip in efficiency in the range  $55700 \lesssim \text{MJD} \lesssim 55800$  is due to overly aggressive filtering of false detections during that time period. The fit to the limiting magnitude in each passband as a function of time is consistent with there being no change in any filter.

In Fig. 25 we compare the predicted number of tracklets using the S3M to Pan-STARRS1 tracklets reported to the MPC during the period 13 Aug 2011 through 11 Oct 2011. For bright main-belt asteroids with  $w_{P1} < 19$ , Pan-STARRS1 reported about 1/3 the predicted number. Fainter than  $w_{P1} = 19$  the reported rate drops further until the sensitivity limit is reached. Many factors account for the discrepancy between the predicted

and realized rates:

1. objects can be lost (primarily MBOs) in image differencing when observing away from opposition because of stationary points (*i.e.* the differencing subtracts all or part of the detection)
2. tracklets submitted to the MPC might not yet be assigned a designation (a ‘one night stand’ tracklet)
3. per-exposure live detector fraction may fall below the nominal 75% due to *e.g.* aggressive masking in regions with high stellar sky-plane density
4. true night-to-night sensitivity in  $w_{P1}$  is poorer than the constant model used for synthetics
5. the synthetic  $S/N$  model overestimates faint-end performance
6. the S3M may overstate the number of objects in some sub-populations.

The situation is better for the NEOs that show better agreement between the model and Pan-STARRS1 down to the sensitivity limit. The effect of (1) almost disappears because NEOs will rarely have stationary sky-plane motion, and (2) is reduced because of the NEO confirmation process for one-night tracklets coordinated by the MPC.

## 6. Current Pan-STARRS1 Performance

As of late 2012, great strides have been made image processing and telescope scheduling to increase the yield of asteroids from the Pan-STARRS1 survey. Better measurement and modeling of detector readout noise has resulted in greater detection sensitivity in image processing. Finer characterization of detection morphology by the IPP allows MOPS to

reject many classes of false detections upon ingest so that they do not contaminate the NEO tracklet review process. The Pan-STARRS1 Modified Design Reference Mission survey (Chambers 2012) has increased the fraction of  $3\pi$  survey time spent observing in quads. With the recent completion of the  $3\pi$  static sky processing, there will be additional improvement in the system limiting magnitude of at least 0.4 mag as IPP moves from pairwise difference imaging to static sky differencing.

Fig. 26 shows NEO discovery and submitted object totals for Pan-STARRS1 and other NEO surveys. Although monthly totals can vary with weather losses, since late 2010 the Pan-STARRS1 NEO discovery rate has been increasing. Using IPP’s morphological characterization and a MOPS comet candidate review procedure similar to that for NEOs, Pan-STARRS1 has become a capable comet finder, discovering 30 to date and 8 in October 2012 alone.

## 7. Availability & Ongoing Development

The MOPS software is available under the GNU General Public License Version 2, and can be retrieved by sending a query to the PS1 Science Consortium (<http://www.ps1sc.org>). MOPS has become a large and somewhat unwieldy package, employing (too many) different programming languages preferred by third-party software (not all available directly from the PS1SC), and containing many installation dependencies for Perl and Python modules. Fortunately, documentation and development notes are available via the PS1SC web site.

Not all MOPS subcomponents are freely available and some are not integrated into the MOPS software distribution. In particular, the JPL Solar System Dynamics package that performs MOPS differential correction must be obtained directly from JPL. Other

packages such as OrbFit and the SLALIB positional astronomy library must be downloaded separately.

Approximately 15-20 full-time equivalent (FTE) years have gone into the development of MOPS and the S3M, and development continues in support of Pan-STARRS1’s ongoing NEO survey and upcoming NEO surveys such as ATLAS (Tonry et al. 2012). Prior to handling live Pan-STARRS1 data, MOPS processed testing data from Spacewatch (*e.g.* Gehrels 1991; Gehrels and Jedicke 1996) and raw data in support of the Thousand Asteroid Light Curve Survey (TALCS; Masiero et al. 2009). MOPS has additionally been instrumental in providing simulation results for Pan-STARRS, LSST and ATLAS, and as a research tool for many graduate students and postdocs.

## 8. Future improvements

The future of MOPS likely falls in several areas:

- Optimizing execution speed for next-generation Pan-STARRS4-like data volumes through reduction of database I/O and greater in-memory processing.
- Improved MOPS installation and configuration for non-Pan-STARRS surveys.
- Modeling of photometric artifacts, *e.g.* partially masked PSFs and trails.
- The linear processing model employed by MOPS is appropriate for a mature survey but can be inadequate when evaluating production parameters. It is difficult to merge separate MOPS databases created under different runtime configurations into a single coherent database. Future versions of MOPS should be more agile in its ability to perform non-linear processing and merge datasets.

- Increased fidelity of synthetics. For example, although our simulations coarsely avoid the moon they do not incorporate the effects of varying sky sensitivity or effects due to the presence of bright objects in the field of view. In one sense, however, these effects are really an aspect of detector sensitivity and not MOPS itself, and they can be integrated via per-field detection efficiency parameters if they are measured by IPP.
- Fill-factor modeling. There is experimental code to use the mask of Fig. 6 as a crude live-pixel server (LPS, §3.12) to simulate detections lost on dead areas of the detector.
- Simplified processing for large-scale simulations, *e.g.* two-body ephemerides instead of a perturbed dynamical model.

## 9. Summary

MOPS has proven to be a capable tool for detecting moving objects in the Pan-STARRS1 transient detection stream. Despite the differences between the targeted Pan-STARRS4 capability and current Pan-STARRS1 performance, we have deployed MOPS effectively in our search for NEOs and comets and in characterizing the main belt. Importantly, we have estimates of our efficiency of object detection so that we can provide a foundation for large-scale population studies.

Additionally, we have made progress toward our design goal of creating a system that can detect objects and compute their orbits with  $> 99\%$  efficiency for most solar system populations when provided next-generation survey astrometry and data quality. Our experience with Pan-STARRS1 shows that the desired performance is challenging to achieve with real telescope data.

With nearly one year remaining in the Pan-STARRS1 survey, we expect further

broad improvements in astrometry, photometry, difference imaging and sensitivity in the final Pan-STARRS1 data release. The Pan-STARRS2 telescope (Burgett 2012) is under construction adjacent to the Pan-STARRS1 facility and will have a raw detector sensitivity and optical performance exceeding that of Pan-STARRS1. Operating modes currently under consideration for the two telescopes have them working in tandem, increasing performance even further. Combined with optimization and tuning of the Pan-STARRS1 MOPS pipeline, we look forward to applying the full capability of MOPS to this data and to the subsequent riches that will lie in this catalog of moving objects.

### **Acknowledgments**

The Pan-STARRS1 Survey has been made possible through contributions of the Institute for Astronomy, the University of Hawai'i, the Pan-STARRS Project Office, the Max-Planck Society and its participating institutes, the Max Planck Institute for Astronomy, Heidelberg and the Max Planck Institute for Extraterrestrial Physics, Garching, The Johns Hopkins University, Durham University, the University of Edinburgh, Queen's University Belfast, the Harvard-Smithsonian Center for Astrophysics, and the Las Cumbres Observatory Global Telescope Network, Incorporated, the National Central University of Taiwan, and the National Aeronautics and Space Administration under Grant No. NNX08AR22G issued through the Planetary Science Division of the NASA Science Mission Directorate.

The design and construction of the Panoramic Survey Telescope and Rapid Response System by the University of Hawaii Institute for Astronomy was funded by the United States Air Force Research Laboratory (AFRL, Albuquerque, NM) through grant number F29601-02-1-0268.



We thank the Jet Propulsion Laboratory, an operating division of the California Institute of Technology, for providing an executable version of their Rapid Comet and Asteroid Orbit Determination Process software (NTR-41180) to the Institute for Astronomy at the University of Hawai'i for use in MOPS.

We acknowledge the financial and technical contributions to this work made by the Large Synoptic Survey Telescope (LSST) Corporation team, in particular Tim Axelrod, Lynne Jones and Jeff Kantor. In addition, we acknowledge the support by Pan-STARRS and LSST management to enable and facilitate this productive collaborative effort between the two projects.

Don Yeomans (JPL) and Ted Bowell (Lowell Observatory) provided expert feedback as external reviewers for the MOPS system in the early years of its development.

Many colleagues provided helpful feedback on the MOPS system operation and usability as well as supporting MOPS development. We would in particular like to thank Wen-Ping Chen and Rex Chang from the Institute of Astronomy, National Central University, Taiwan.

This research has made use of the SIMBAD database, operated at CDS, Strasbourg, France.

Table 1. MOPS Pan-STARRS1 Filter Transformations\*

Transform	Solar	Mean S+C	$t_{exp}$ (s) †
$V-g_{P1}$	-0.217	-0.28	43
$V-r_{P1}$	0.183	0.23	40
$V-i_{P1}$	0.292	0.39	45
$V-z_{P1}$	0.311	0.37	30
$V-y_{P1}$	0.311	0.36	30
$V-w_{P1}$	0.114	0.16	45

Note. — Transformations from Johnson  $V$  to the six Pan-STARRS filters are provided for both a standard solar spectrum and asteroids with a mean S+C spectral type. These transformations have been implemented by the Minor Planet Center and AstDyS.

\*Tonry et al. (2012).

†Exposure times as of October 2012.

Table 2. Pan-STARRS1 MOPS Hardware Components (see Fig. 2)

Item	Purpose	Number	Total Capacity
Disk	Database Storage	$2 \times 10$ TB	20 TB <sup>1</sup>
Disk	Administrative	$2 \times 2.7$ TB	5.4 TB
CPU	Cluster processing	$8 \times 4$ cores	32 cores ( $\sim 100$ GFLOPS)
CPU	Administrative <sup>2</sup>	$2 \times 4$ cores	8 cores ( $\sim 25$ GFLOPS)
Network Switch	Network	32 ports	1 Gbps/port

<sup>1</sup>All database storage employs RAID6 for data integrity.

<sup>2</sup>Administrative functions include a user console, pipeline and Condor workflow management, and the web interface.

Table 3. MOPS Database Storage Requirements

Data Component	PS4 Estimated (GB)	PS1 Estimated (GB)	PS1 Actual <sup>1</sup> (GB)
Fields	0.2	0.06	0.02
$3\sigma$ Detections	500,000	150,000	N/A <sup>2</sup>
$5\sigma$ Detections	500	150	122
Derived Object Parameters	1,000	300	0.152 <sup>3</sup>
Synthetic Object Parameters	1,100	330	2.43 <sup>4</sup>
Tracklets	1,200	360	2.19 <sup>5</sup>
Image Postage Stamps	N/A	N/A	1,800 <sup>6</sup>

<sup>1</sup>As of October 2012, 2.5 years into the 3.5-year Pan-STARRS1 survey.

<sup>2</sup>Processing of transients below  $3\sigma$  confidence is currently untenable for Pan-STARRS1 MOPS due to the systematic false tracklet rate.

<sup>3</sup>MOPS produces derived object parameters for only a small subset of Pan-STARRS1 data until the pipeline can be tuned for Pan-STARRS1 performance.

<sup>4</sup>Pan-STARRS1 operations uses a 1/10 sampled synthetic solar system model (S3M). A final Pan-STARRS1 processing of its transient catalog will include a full S3M.

<sup>5</sup>Pan-STARRS1 single-exposure sensitivity reduces the actual tracklet count on top of the reduction from a shorter survey than Pan-STARRS4.

<sup>6</sup>Image postage stamps ( $200\times 200$  pixels) are stored on a network file system, not in the MOPS database. They are locatable using database records.

Table 4. S3M Grid Model Semi-Major Axis Number Distribution (see Fig. 7).

Semi-major axis range (AU)	Number of objects
0.75-1.5	50,000
1.5-6.0	200,000
6.0-32	50,000
32-50	200,000
50-500	50,000
500-5000	25,000

Note. — The number of objects in each pseudo-logarithmic range and their absolute magnitudes were selected so that the sky-plane density of detected objects in the simulations will be similar.

Table 5. Tracklet (intra-night) Efficiency\* & Accuracy\* in the 2-year Pan-STARRS4 MOPS full-density simulation.

Avail.	Clean	%	Unfound	%	Mixed	%	Bad	%	Non-syn.
24056199	24056191	100.0	8	0.0	417774	1.7	553475	2.3	1854648

Note. — This simulation used a realistic solar system model (S3M) and “next-generation” (0.01”) astrometric uncertainty (about 10× better than delivered by the best contemporary surveys like Pan-STARRS1). The tracklet terminology in the headings is described in detail in §3.11.

\*See §3.1 and §3.11 for definitions of efficiency and accuracy.

Table 6. Derived Object Efficiency for eight<sup>†</sup> different classes of synthetic solar system objects in the 2-year Pan-STARRS4 MOPS full-density simulation.

Object Class <sup>1</sup>	Avail.*	Clean* (Linked)	%	Pass IOD <sup>2</sup>	%	Pass Diff. <sup>3</sup>	%
NEO	5203	4994	96.0	4924	94.6	4924	94.6
MBO	2043584	2032676	99.5	2029618	99.3	2029618	99.3
TRO	56214	56061	99.7	55923	99.5	55923	99.5
CEN	557	556	99.8	556	99.8	556	99.8
JFC	551	546	99.1	541	98.2	541	98.2
LPC	1714	1713	99.9	1584	92.4	1584	92.4
SDO	2289	2286	99.9	2281	99.7	2281	99.7
TNO	12719	12710	99.9	12686	99.7	12686	99.7

Note. — This simulation used a realistic solar system model (S3M) and “next-generation” (0.01”) astrometric uncertainty (about 10× better than delivered by the best contemporary surveys like Pan-STARRS1). The tracklet terminology in the headings is described in detail in §3.11.

\*See §3.1 and §3.11 for definitions of efficiency and accuracy.

<sup>†</sup>The impactor and hyperbolic models are omitted because they did not exist in the S3M at the time of this simulation.

<sup>1</sup>NEO - Near Earth Objects; MBO - Main Belt Objects; TRO - Trojans; JFC - Jupiter Family Comets; LPC - Long Period Comets; CEN - Centaurs; SDO - Scattered Disk Objects; TNO -

## Trans-Neptunian Objects

<sup>2</sup>the number (and percentage) for which initial orbit determination was successful.

<sup>3</sup>the number (and percentage) for which a differentially corrected orbit was successfully computed.



Table 7. Derived Object Efficiency for the 4-year Pan-STARRS1 MOPS NEO-only simulation.

Object Class <sup>1</sup>	Avail.*	Clean* (Linked)	%	Pass IOD <sup>1</sup>	%	Pass Diff. <sup>2</sup>	%
NEO	11515	11025	95.7	9404	81.7	9404	81.7

Note. — This simulation used a realistic population of  $\sim 250,000$  NEOs with Pan-STARRS1-like astrometric uncertainty ( $0.1''$ ) simulation and a 100% fill-factor detector. This simulation was run during commissioning of the Pan-STARRS1 telescope before the actual Pan-STARRS1 survey was implemented.

\*See §3.1 and §3.11 for definitions of efficiency and accuracy.

<sup>1</sup>the number (and percentage) for which initial orbit determination was successful.

<sup>2</sup>the number (and percentage) for which a differentially corrected orbit was successfully computed.

Table 8. Tracklet Efficiency\* & Accuracy\* in Pan-STARRS1 Observing Cycle 143  
(2011-08-13 through 2011-09-10)<sup>†</sup>.

Avail.	Clean	%	Unfound	%	Mixed	%	Bad	%	Non-syn.
246596	246558	100.0	38	0.0	1969	0.8	8884	3.6	1429073

Note. — Measured performance for a single observing cycle of real Pan-STARRS1 telescope pointings using realistic astrometric uncertainty (0.1'') and a simplistic 75% fill-factor model.

\*See §3.1 and §3.11 for definitions of efficiency and accuracy.

<sup>†</sup>Excluding fields within 15° of the Galactic Plane.

Table 9. Cumulative derived object efficiency for 10 different classes of synthetic solar system objects in Pan-STARRS1 Observing Cycle 143 (2011-08-13 through 2011-09-10).<sup>†</sup>

Object Class <sup>1</sup>	Avail.*	Clean* (Linked)	%	Pass IOD <sup>2</sup>	%	Pass Diff. <sup>3</sup>	%	Dup. <sup>4</sup>	%
IMP	88	68	77.3	67	76.1	67	76.1	0	0.0
NEO	24	18	75.0	18	75.0	18	75.0	0	0.0
MBO	18301	14608	79.8	14551	79.5	14461	79.0	6	0.0
TRO	662	538	81.3	538	81.3	522	78.9	0	0.0
CEN <sup>5</sup>	0	0	0.0	0	0.0	0	0.0	0	0.0
JFC	22	18	81.8	18	81.8	18	81.8	0	0.0
LPC	50	39	78.0	36	72.0	36	72.0	0	0.0
SDO	7	1	14.3	1	14.3	1	14.3	0	0.0
TNO	17	15	88.2	15	88.2	15	88.2	0	0.0
HYP	32	27	84.4	19	59.4	19	59.4	0	0.0

Note. — Measured performance for a single observing cycle of real Pan-STARRS1 telescope pointings using realistic astrometric uncertainty (0.1'') and a simplistic 75% fill-factor model.

\*See §3.1 and §3.11 for definitions of efficiency and accuracy.

<sup>†</sup>Excluding fields within 15° of the galactic equator.

<sup>1</sup>IMP - Earth Impactor; NEO - Near Earth Objects; MBO - Main Belt Objects; TRO - Trojans; JFC - Jupiter Family Comets; LPC - Long Period Comets; CEN - Centaurs; SDO - Scattered Disk

Objects; TNO - Trans-Neptunian Objects; HYP - Hyperbolic (Interstellar) Objects

<sup>2</sup>the number (and percentage) for which initial orbit determination was successful.

<sup>3</sup>the number (and percentage) for which a differentially corrected orbit was successfully computed.

<sup>4</sup>the number (and percentage) of duplicate derivations. The duplicates contain non-identical but intersecting sets of detections of the same object.

<sup>5</sup>Centaurids were inadvertently omitted from the S3M for this study.

Table 10. Attribution Efficiency\* & Accuracy\* in Pan-STARRS1 Observing Cycle 143  
(2011-08-13 through 2011-09-10).<sup>†</sup>

Avail.*	Clean*	%	Mixed*	%	Bad*	%	Non-syn.*
9684	8971	92.6	5	0.1	26	0.3	3625

Note. — Measured performance for a single observing cycle of real Pan-STARRS1 telescope pointings using realistic astrometric uncertainty ( $0.1''$ ) and a simplistic 75% fill-factor model.

\*See §3.1 and §3.11 for definitions of efficiency and accuracy.

<sup>†</sup>Excluding fields within  $15^\circ$  of the Galactic Plane.

Table 11. MOPS Precovery Efficiency\* & Accuracy\* in Pan-STARRS1 Observing Cycle  
143 (2011-08-13 through 2011-09-10).<sup>†</sup>

Avail.*	Clean*	%	Mixed*	%	Bad*	%	Non-syn*
8557	6635	77.5	14	0.2	23	0.3	1966

Note. — Measured performance for a single observing cycle of real Pan-STARRS1 telescope pointings using realistic astrometric uncertainty ( $0.1''$ ) and a simplistic 75% fill-factor model.

\*See §3.1 and §3.11 for definitions of efficiency and accuracy.

<sup>†</sup>Excluding fields within  $15^\circ$  of the galactic equator.

Table 12. Orbit Identification Matching Tolerances

---

---

Orbit Element <sup>1</sup>	Tolerance
perihelion	0.1 AU
eccentricity	0.05
inclination	0.1°
ascending node	1°
arg. of perihelion	1°
time of perihelion <sup>2</sup>	0.1

---

Note. — The maximum difference between two derived object’s orbits before they are tested for consistency with being the same object.

<sup>1</sup>Cometary form.

<sup>2</sup>In terms of fractional orbit period.

Table 13. MOPS Orbit Identification Efficiency\* & Accuracy\* in Pan-STARRS1  
Observing Cycles 143 & 144 (2011-08-13 through 2011-10-10).<sup>†</sup>

Avail.*	Found*	%	Mixed*	%	Bad*	%	Non-syn.
40	7	17.5	1	2.5	2	5.0	22

Note. — Measured performance for a single observing cycle of real Pan-STARRS1 telescope pointings using realistic astrometric uncertainty ( $0.1''$ ) and a simplistic 75% fill-factor model.

\*See §3.1 and §3.11 for definitions of efficiency and accuracy.

<sup>†</sup>Excluding fields within  $15^\circ$  of the galactic equator.



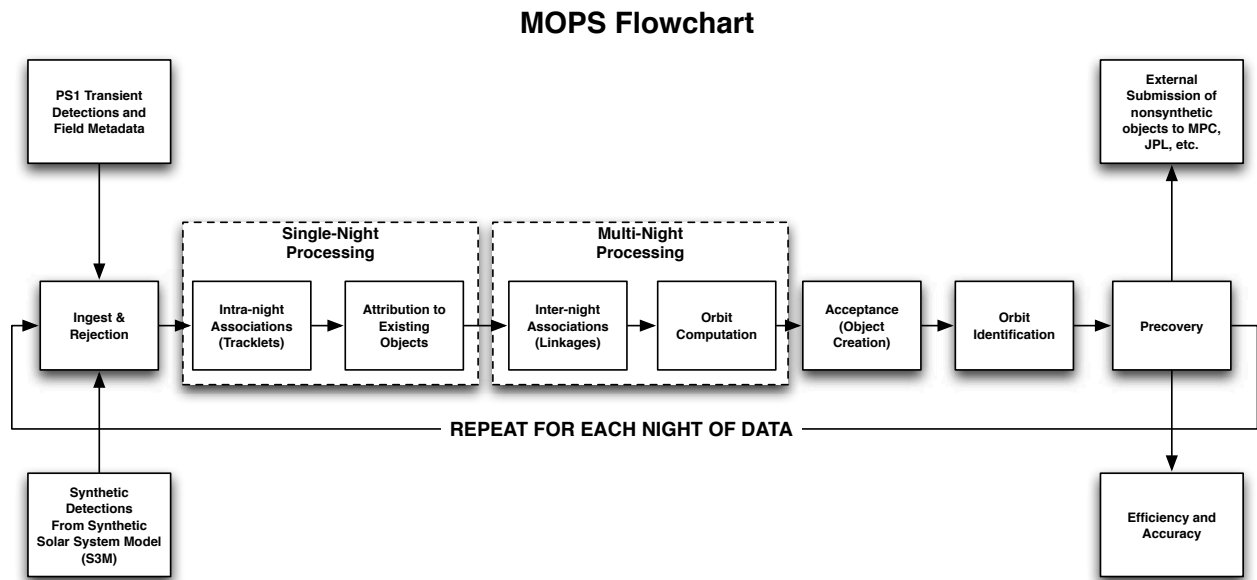


Fig. 1.— High level flowchart for the Pan-STARRS1 Moving Object Processing System (MOPS). The data processing proceeds from left to right in the figure, then repeats for every additional night of data ingested by MOPS.

### MOPS PS1 Cluster Organization

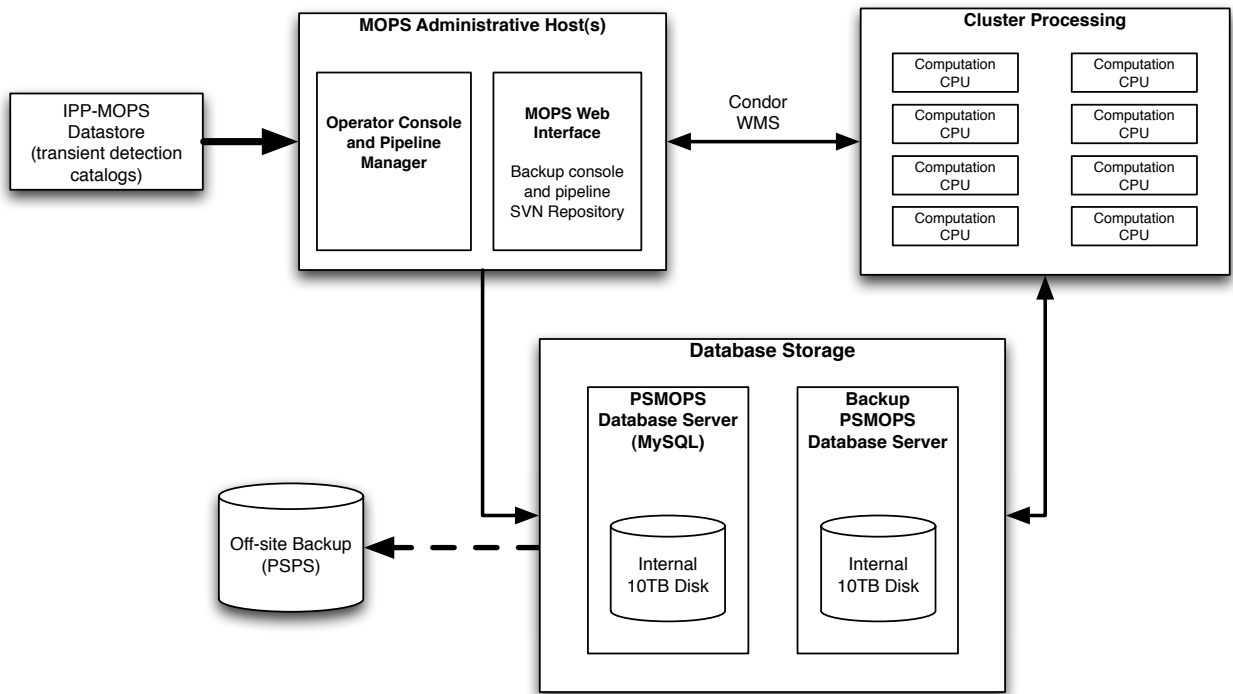


Fig. 2.— MOPS Pan-STARRS1 cluster configuration.

### MOPS Database Design

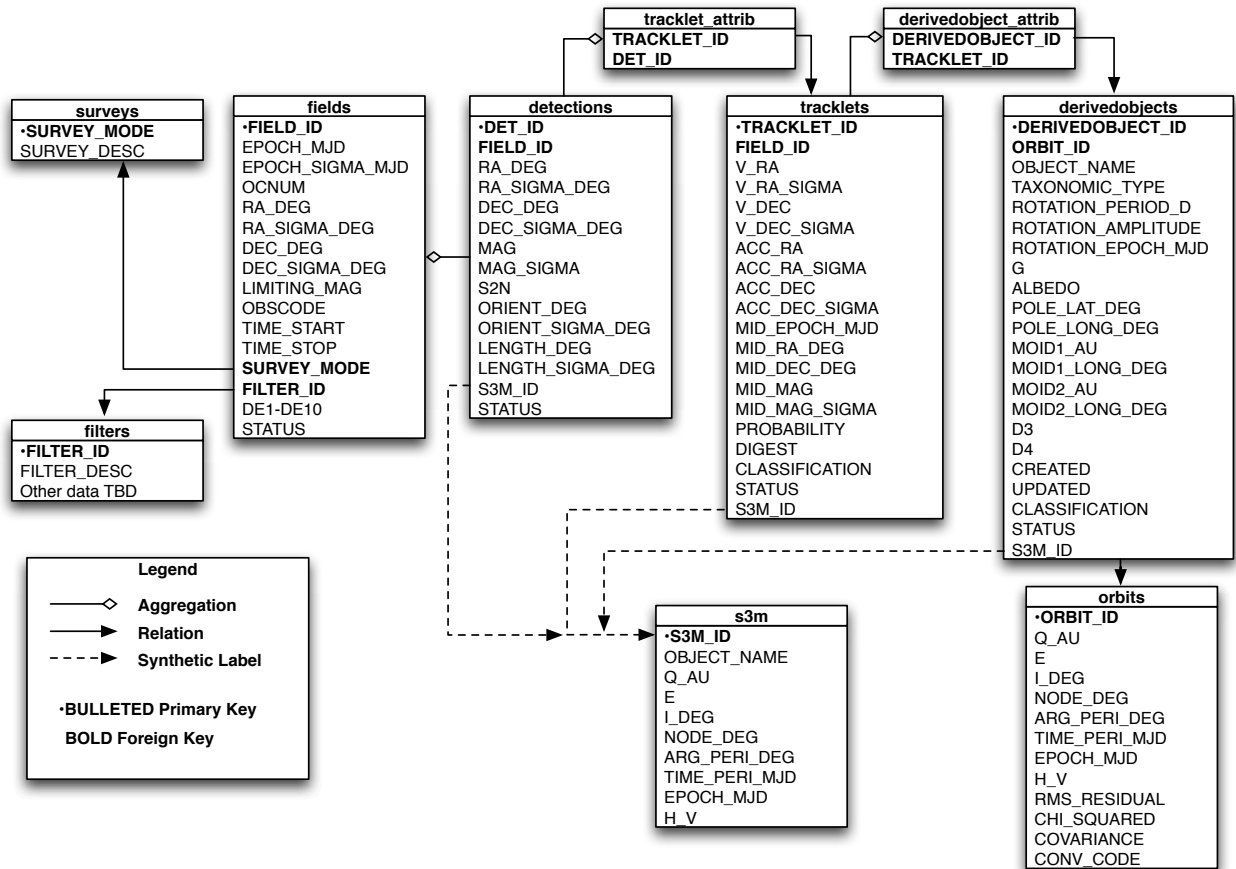


Fig. 3.— MOPS database schema. S3M columns indicate synthetic data for efficiency assessment.

psmops\_ps1\_mdrm152

Configuration | Alerts | Lookup:  Search  
 MJD, TJD, UT date (YYYYMMDD), tracklet ID, derived object name, "today", "latest"  
 MPC Obs Search

Nonsynthetic All | Nonsynthetic NEOs | Known Objects | Tabular (first 100) | Tabular (all) | e vs. a 10AU | 50AU | e vs. q 10AU 50AU

### TJD 6210

WED 10 OCT 2012 UT  
 OC 157

#### All Chunks By Observation Time

Chunk Name	Obs Time (HST)	Last Processing Status	Num Exposures
156.3PI.00.PW+1.J.y	18:44 HST	POSTTRACKLET	28
156.3PI.00.W-4.J.z	19:05 HST	POSTTRACKLET	42
MD09	21:11 HST	POSTTRACKLET	8
157.3PI.00.BNW3.J.g	21:47 HST	POSTTRACKLET	36
157.OSS.A.Q.w	22:24 HST	POSTTRACKLET	84
157.3PI.00.PS.J.g	00:05 HST	POSTTRACKLET	38
157.3PI.00.PN2.J.g	01:08 HST	POSTTRACKLET	20
MD10	01:29 HST	POSTTRACKLET	8
MD01	02:04 HST	POSTTRACKLET	8
MD02	02:39 HST	POSTTRACKLET	8
157.3PI.00.BNE3.J.r	03:15 HST	TRACKLET	38
157.3PI.00.BNE3.J.i	03:49 HST	TRACKLET	38
156.3PI.00.E-4.K.z	04:27 HST	INGESTED	44
157.3PI.00.E-3.K.z	05:01 HST	INGESTED	2
157.3PI.00.E-3.K.y	05:22 HST	INGESTED	22

#### By Run ID

Run 259 updated 2012-10-10 08:58:40

Chunk Name	Type	Status	Footprints
157.3PI.00.BNE3.J.i	QUAD	TRACKLET	19

Run 258 updated 2012-10-10 06:35:03

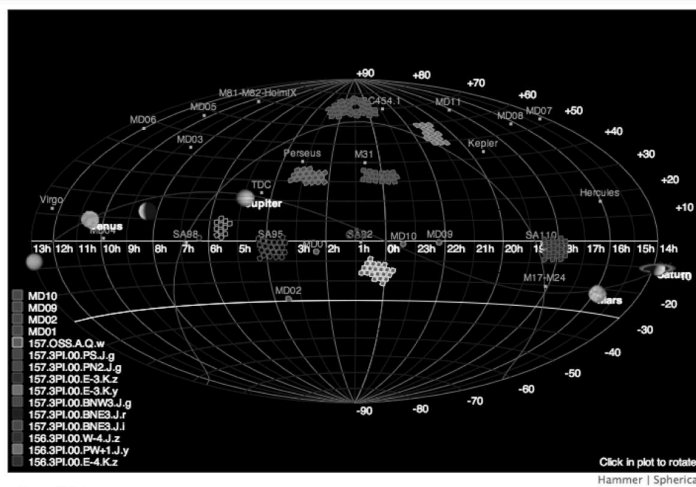
Chunk Name	Type	Status	Footprints
MD10	MD	POSTTRACKLET	1
156.3PI.00.PW+1.J.y	PAIR	POSTTRACKLET	14
156.3PI.00.W-4.J.z	PAIR	POSTTRACKLET	21
157.3PI.00.BNW3.J.g	PAIR	POSTTRACKLET	18
157.3PI.00.PN2.J.g	PAIR	POSTTRACKLET	10
157.3PI.00.PS.J.g	PAIR	POSTTRACKLET	19

Run 257 updated 2012-10-10 05:14:31

Chunk Name	Type	Status	Footprints
157.OSS.A.Q.w	QUAD	POSTTRACKLET	21
MD01	MD	POSTTRACKLET	1
MD02	MD	POSTTRACKLET	1

Run 256 updated 2012-10-10 00:34:56

Chunk Name	Type	Status	Footprints
MD09	MD	POSTTRACKLET	1



TJD 6209  
 TUE 09 OCT 2012 UT  
 OC 157

Fig. 4.— Pan-STARRS1 MOPS web interface showing the sky map for the night of MJD 56210. On the left are lists of observing blocks executed by the telescope for the night.

## MOPS Solar System Processing

All Datasets | Wiki | Admin | Testing | Bugzilla | SVN | Docs | Schema | Submissions | NEO Discoveries | Alerts | SSTF Milk Cartons

**psmops\_ps1\_mdrm152** Configuration | Alerts | Lookup:

TJD (e.g. 5649), UT date (YYYYMMDD), tracklet ID, derived object name, "today", "latest" Logged in as **denneau**

Nonsynthetic All | Nonsynthetic NEOs | Known Objects | Tabular (first 100) | Tabular (all) | e vs. a 10AU | 50AU | e vs. q 10AU 50AU

### Nonsynthetic Tracklets, 3+ Detections, 157.OSS.A

TJD 6210 (MOPS Night Number 56209)  
2012-10-10UT

Showing 1 through 10 of 3342.  
First | Next 10 | Next   No stamps  | Last

Check All |  Uncheck All

Tracklet ID	digest2 Sort	Source Chunk	$V_{tot}$ (deg/day) Sort	Apparent Mag (V)	Pos Ang (deg) Sort	Known As Sort	Known q	GCR (arcsec) Sort	Probability Sort	Submission Status	Stamps
<b>7358107</b> <small>Review</small>	100.0	157.OSS.A.Q.w	0.800 */day	21.8 V	115.7°	N/A	N/A	0.07°	0.71	<input type="checkbox"/>	
<b>7359055</b> <small>Review</small>	100.0	157.OSS.A.Q.w	0.386 */day	20.9 V	-114.1°	2001 WL15	1.05	0.11°	1.00	P1.04/Vu (T, rjw)	
<b>7359805</b> <small>Review</small>	100.0	157.OSS.A.Q.w	3.616 */day	21.5 V	-68.7°	N/A	N/A	0.13°	0.61	<input type="checkbox"/>	
<b>7359806</b> <small>Review</small>	100.0	157.OSS.A.Q.w	0.608 */day	21.6 V	97.3°	N/A	N/A	0.15°	0.59	<input type="checkbox"/>	
<b>7360478</b> <small>Review</small>	100.0	157.OSS.A.Q.w	1.031 */day	21.2 V	91.5°	N/A	N/A	0.15°	0.58	<input type="checkbox"/>	
<b>7361730</b> <small>Review</small>	100.0	157.OSS.A.Q.w	0.423 */day	22.4 V	75.3°	N/A	N/A	0.18°	0.97	<input type="checkbox"/>	
<b>7362301</b> <small>Review</small>	100.0	157.OSS.A.Q.w	0.799 */day	21.2 V	53.6°	N/A	N/A	0.18°	0.99	P1.04/VV (1, rjw)	
<b>7359861</b> <small>Review</small>	100.0	157.OSS.A.Q.w	1.027 */day	22.1 V	-142.8°	N/A	N/A	0.18°	0.83	<input type="checkbox"/>	
<b>7358945</b> <small>Review</small>	100.0	157.OSS.A.Q.w	0.658 */day	19.9 V	76.8°	N/A	N/A	0.19°	0.73	<input type="checkbox"/>	
<b>7360780</b> <small>Review</small>	100.0	157.OSS.A.Q.w	4.550 */day	22.1 V	-51.9°	N/A	N/A	0.23°	0.83	<input type="checkbox"/>	

Check All |  Uncheck All

Showing 1 through 10 of 3342.  
First | Next 10 | Next   No stamps  | Last

Fig. 5.— Pan-STARRS1 MOPS web interface showing the NEO ‘czar’ page. From this page, NEO candidates can be submitted to the IAU Minor Planet Center. Rows 2 and 7 are 2001 WL<sub>15</sub> and 2012 TN<sub>139</sub> respectively.

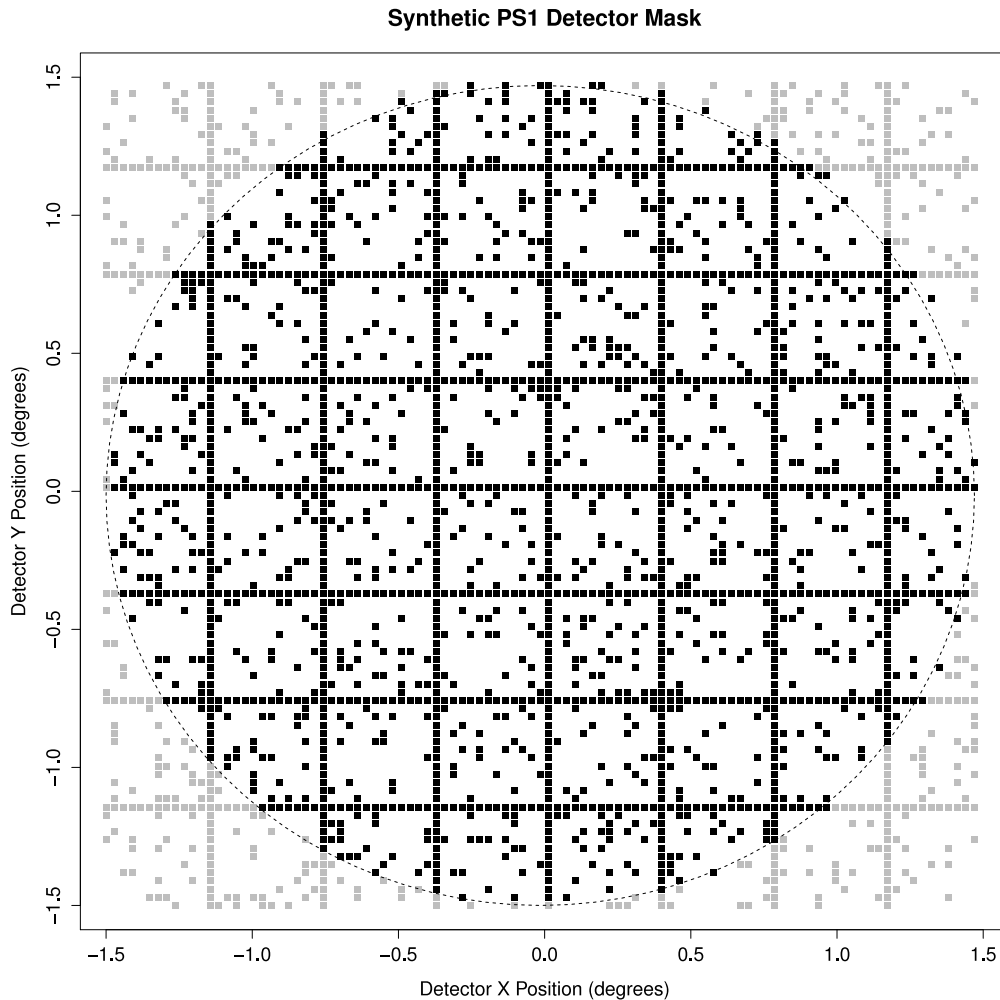


Fig. 6.— Synthetic  $7.0 \text{ deg}^2$  field-of-view static focal plane mask for Pan-STARRS1 MOPS simulations that simulates losses due to chip gaps and other masked area. The horizontal and vertical bands simulate the chip gaps while the remaining squares represent losses due to bad cells or those used for guide stars. The squares do not correspond to actual masked area on the real Pan-STARRS1 detector; they exist simply to simulate additional area loss. The actual distribution of masked area on the real Pan-STARRS1 detector is very different — there is more power on small scales than shown here. The overall simulated camera fill factor is fixed at 75% in agreement with the measured values shown in Fig. 23.

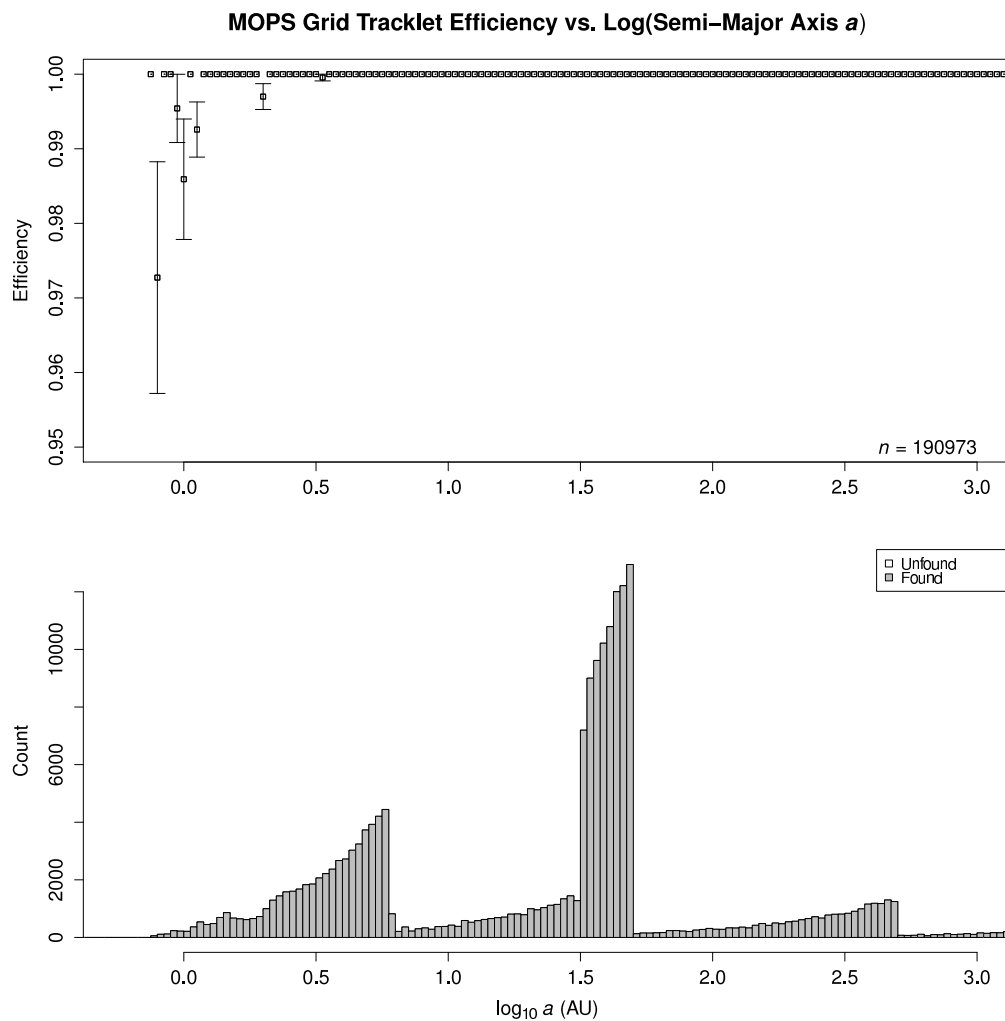


Fig. 7.— Tracklet creation efficiency as a function of semi-major axis for a one lunation MOPS simulation using S3M grid objects. Note the truncated Y-axis range of 0.95 to 1.0. Fifteen fast-moving objects with sky-plane rates that exceed the configured limits for the production Pan-STARRS1 MOPS account for the reduced efficiency at small semi-major axis. These limits will be tuned upon reprocessing the full Pan-STARRS1 survey.

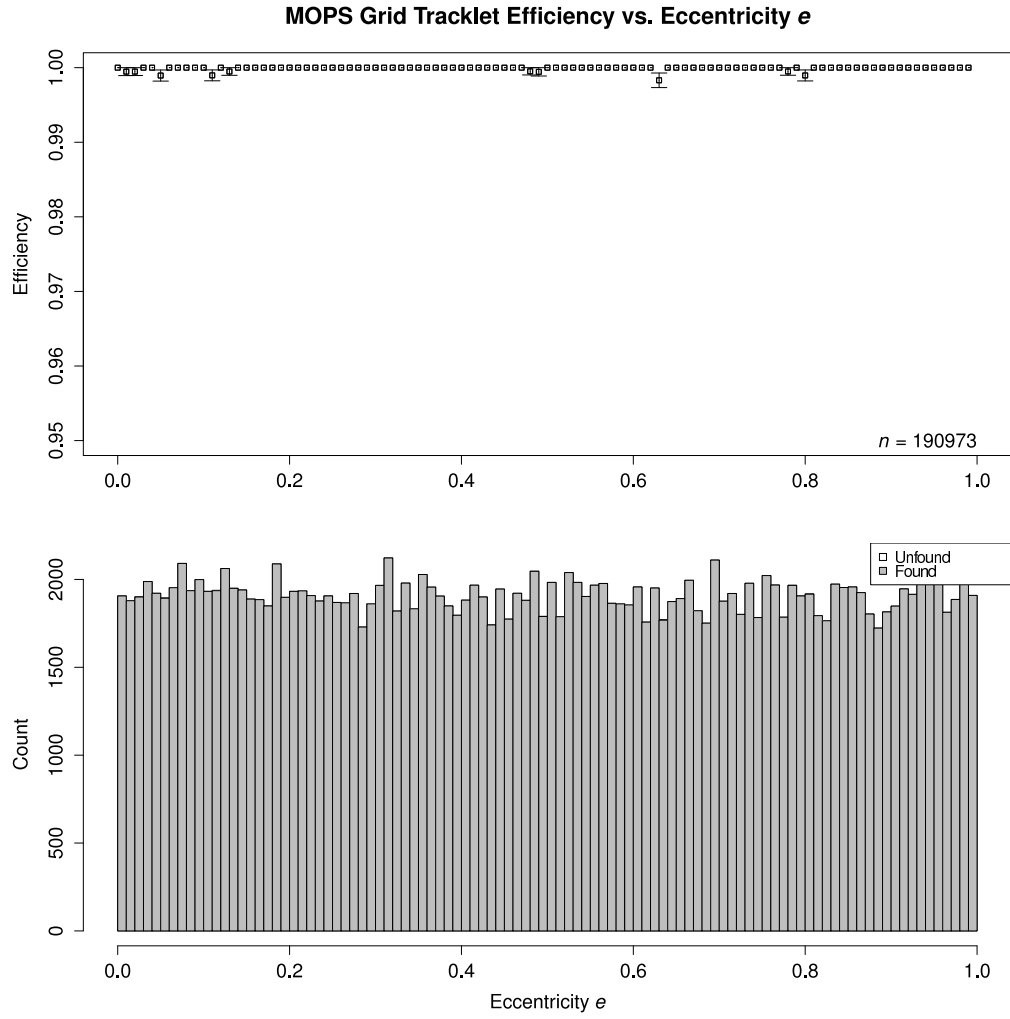


Fig. 8.— Tracklet creation efficiency as a function of eccentricity for a one lunation MOPS simulation using S3M grid objects. Note the truncated Y-axis range of 0.95 to 1.0.



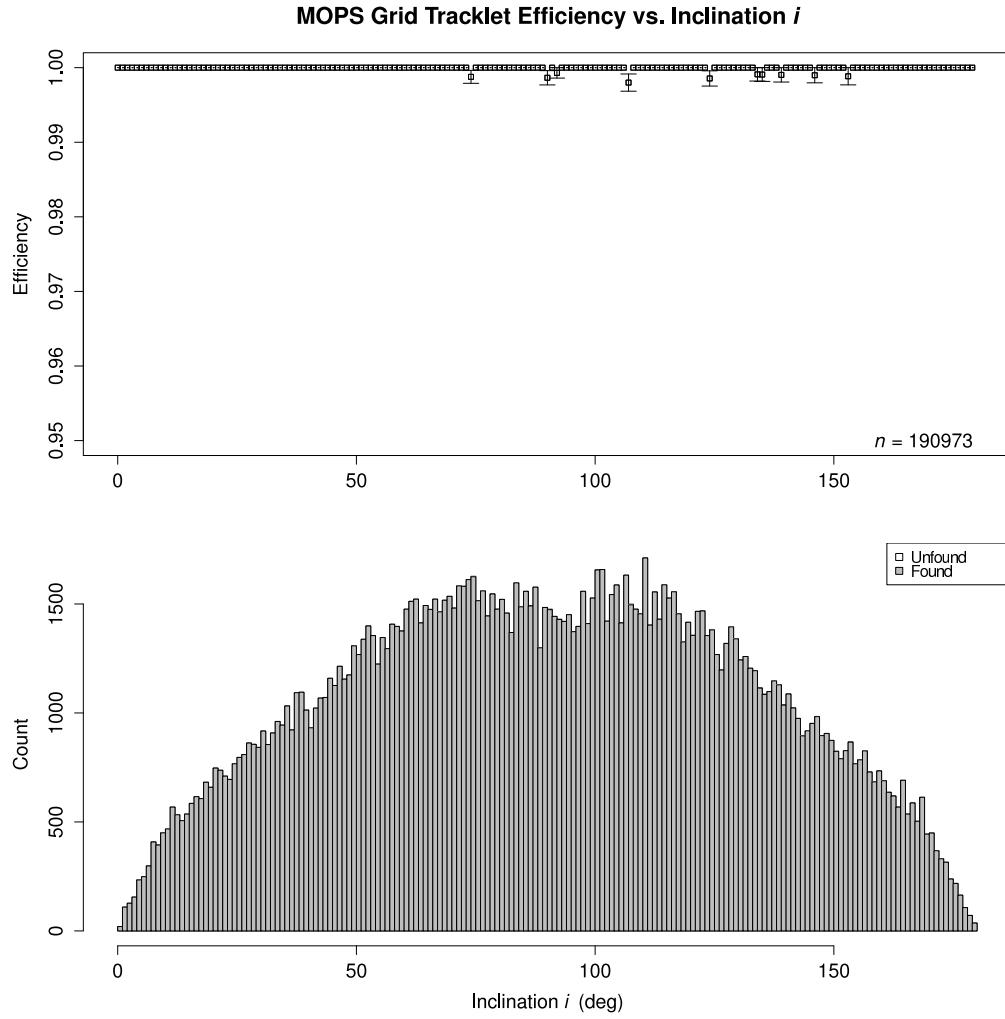


Fig. 9.— Tracklet creation efficiency as a function of inclination for a one lunation MOPS simulation using S3M grid objects. Note the truncated Y-axis range of 0.95 to 1.0.

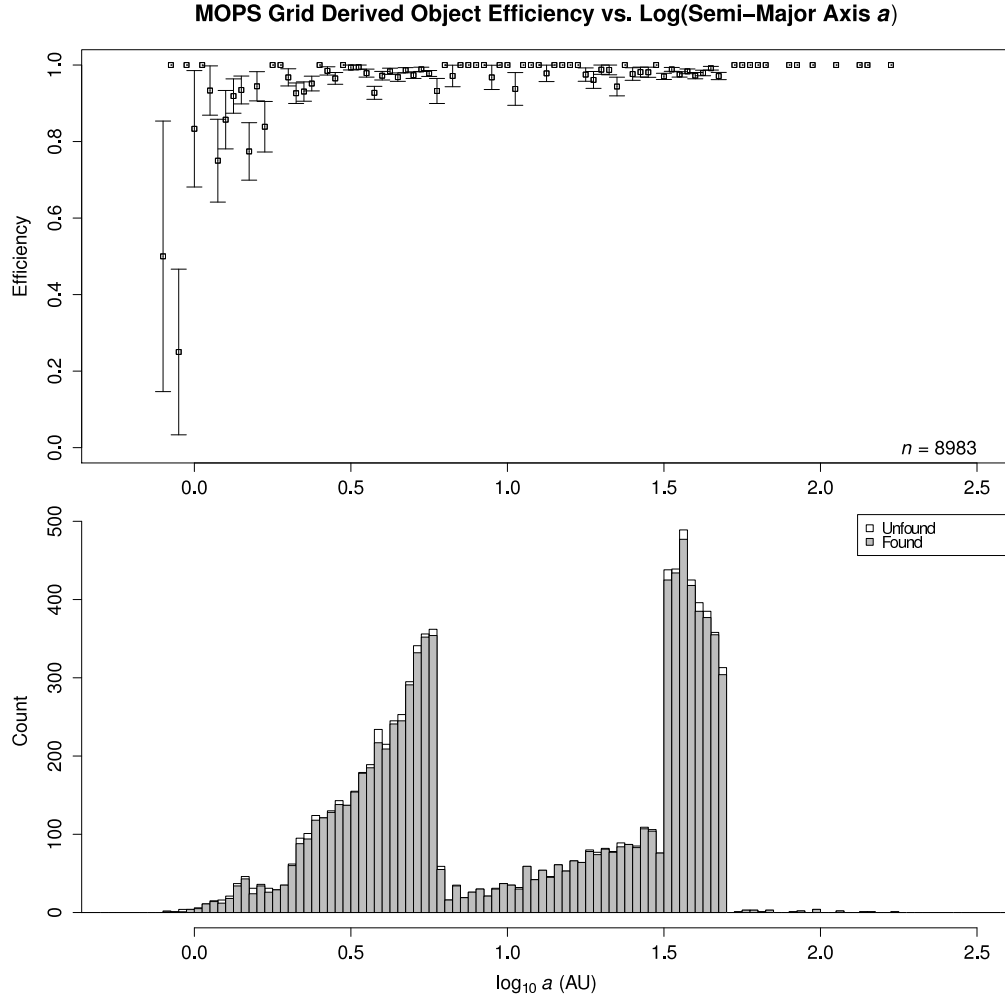


Fig. 10.— Derived object creation efficiency as a function of semi-major axis for a one lunation MOPS simulation using S3M grid objects. The total efficiency is 97.5%. Losses at small semi-major axis are due to conservative acceptance limits in the current Pan-STARRS1 production MOPS that reject objects with large sky-plane accelerations and/or large RMS residuals. These limits will be tuned upon reprocessing the full Pan-STARRS1 survey.

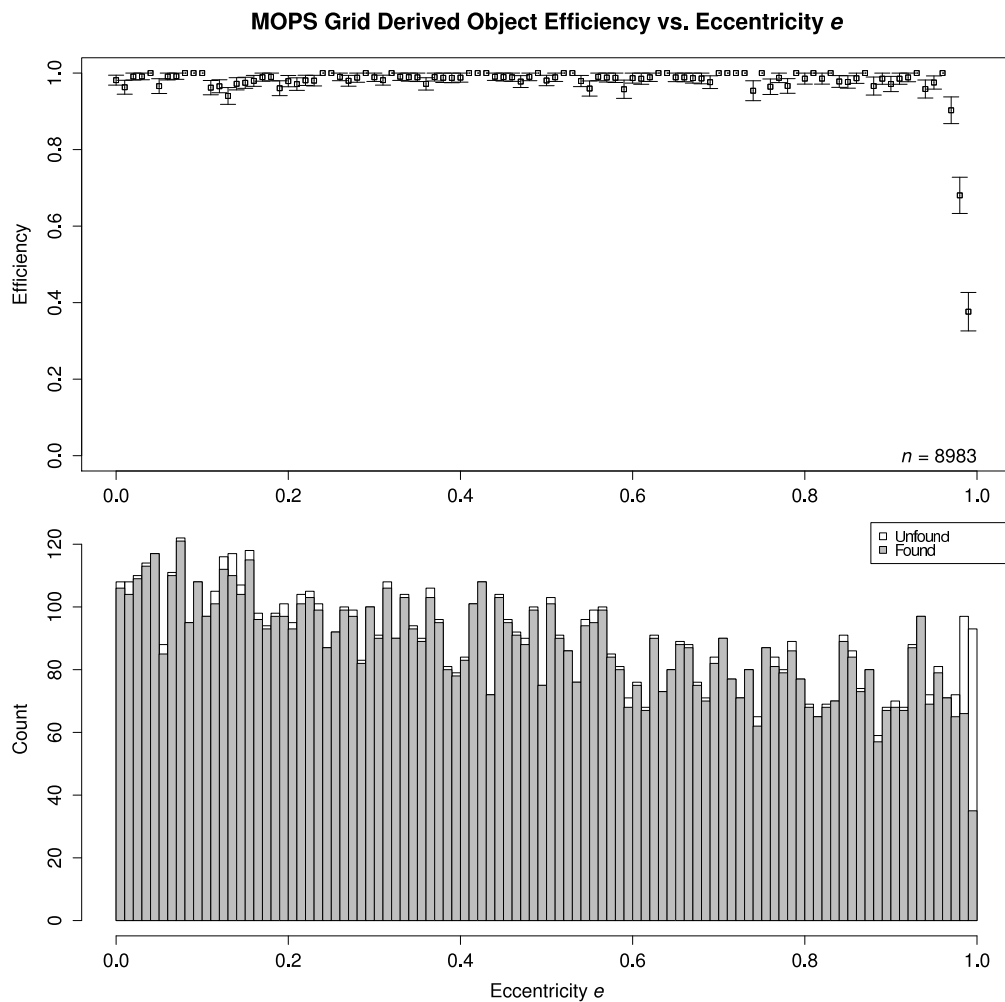


Fig. 11.— Derived object creation efficiency as a function of eccentricity for a one lunation MOPS simulation using S3M grid objects. The failures at high eccentricity ( $e > 0.99$ ) occur in initial orbit determination (IOD) for grid objects with semi-major axis  $a \lesssim 5$ . These failures can be corrected by modifying IOD acceptance parameters.

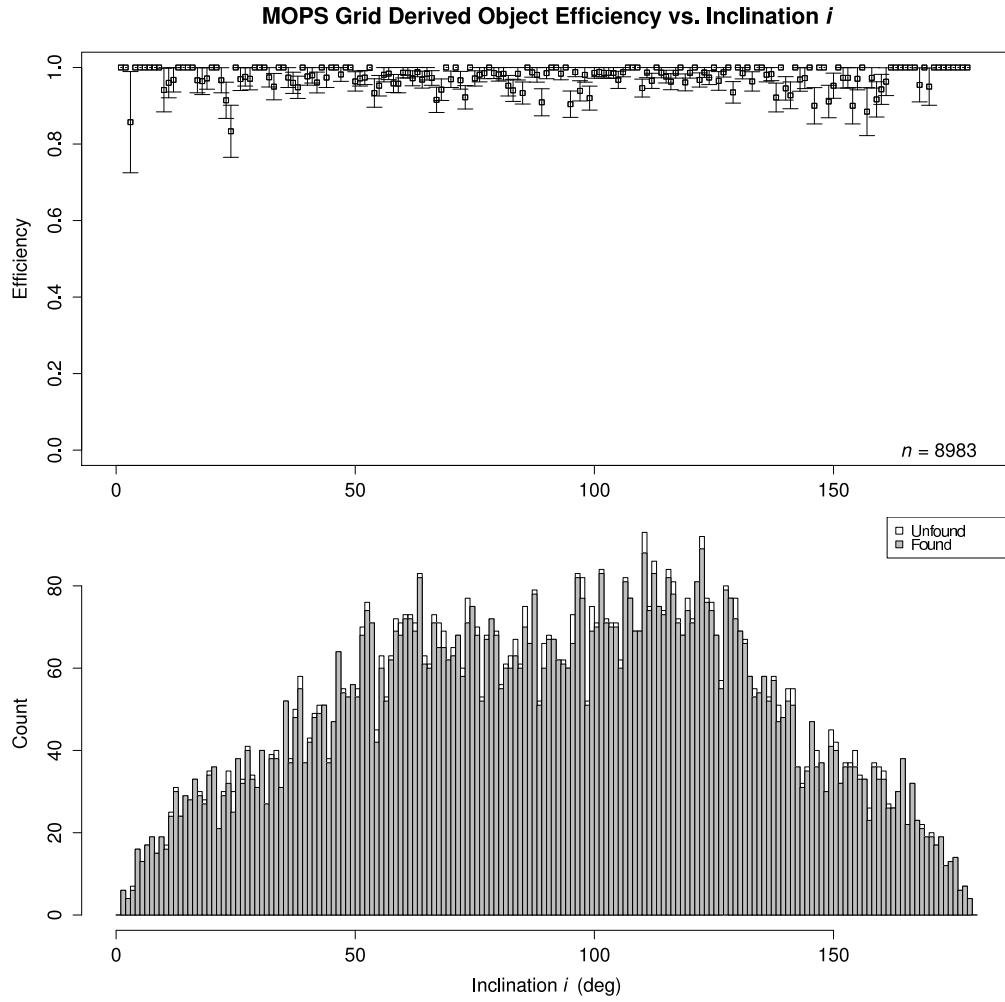


Fig. 12.— Derived object creation efficiency as a function of inclination for a one lunation MOPS simulation using only grid objects.

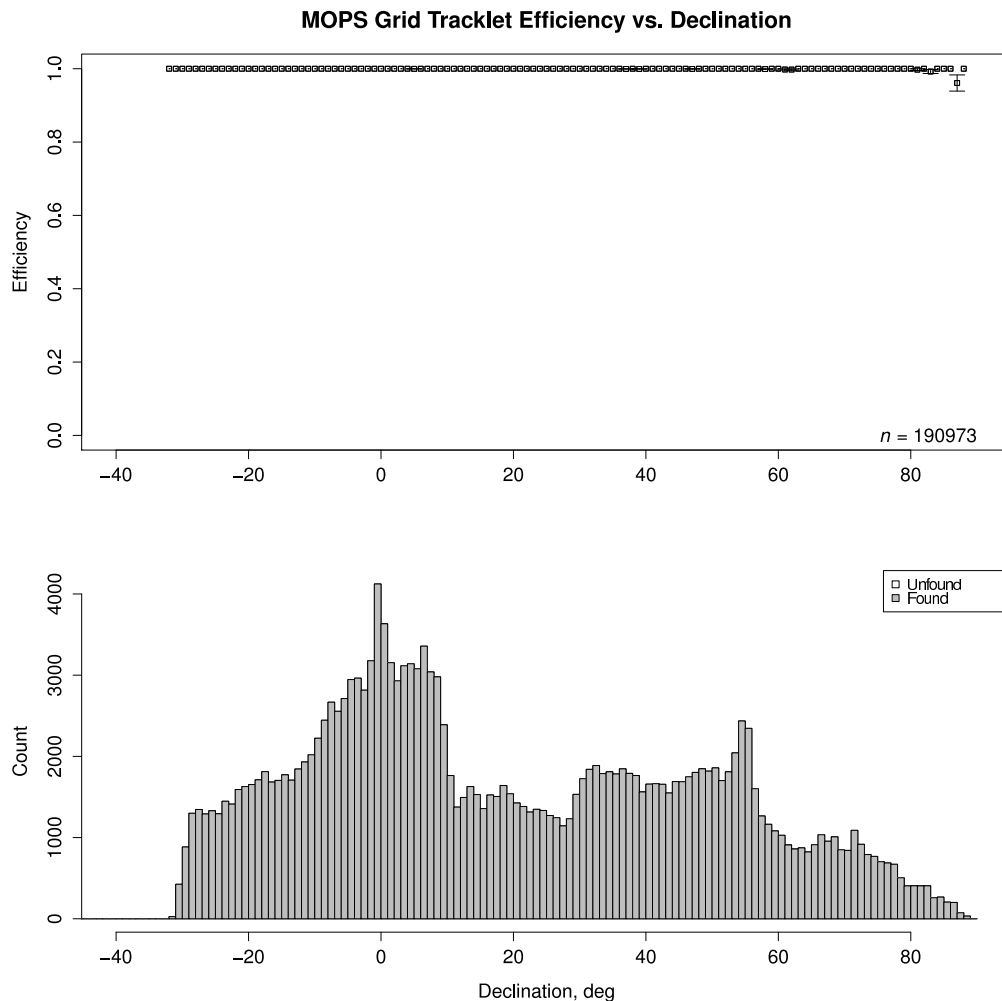


Fig. 13.— Tracklet creation efficiency as a function of declination for a one lunation MOPS simulation using PS1 telescope pointings and S3M grid objects with Pan-STARRS1 realistic ( $0.1''$ ) astrometric uncertainty. The uneven declination coverage is due to uneven coverage of the Pan-STARRS1 survey during the lunation (14 Aug 2011 through 12 Sep 2011). Several fast-moving objects in the declination= $89^\circ$  bin were lost due to overly conservative tracklet acceptance parameters.

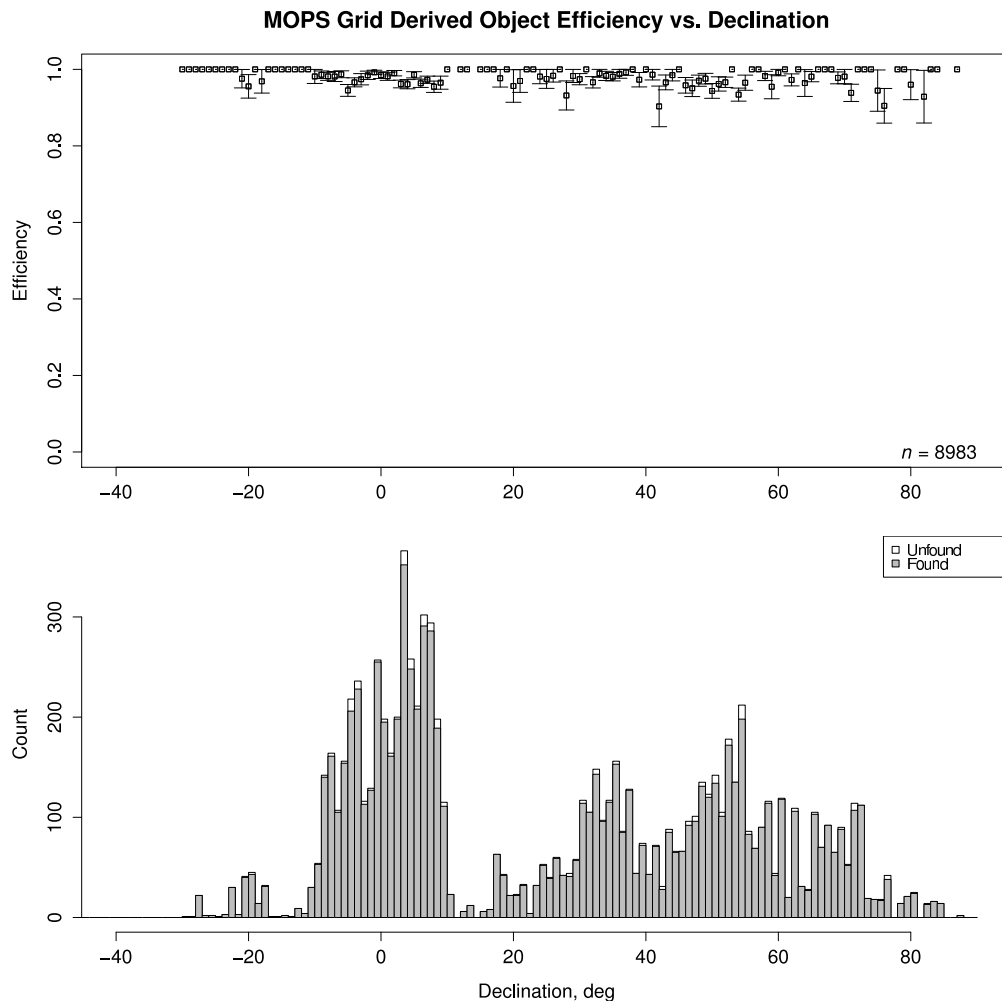


Fig. 14.— Derived object creation efficiency as a function of declination for a one lunation MOPS simulation using S3M grid objects with Pan-STARRS1 realistic ( $0.1''$ ) astrometric uncertainty. The uneven declination coverage is due to uneven multi-night coverage of the Pan-STARRS1 survey during this particular lunation (14 Aug 2011 through 12 Sep 2011). While the total grid derived object efficiency is 97.5%, we believe this number can be improved further by tuning of MOPS linking parameters.

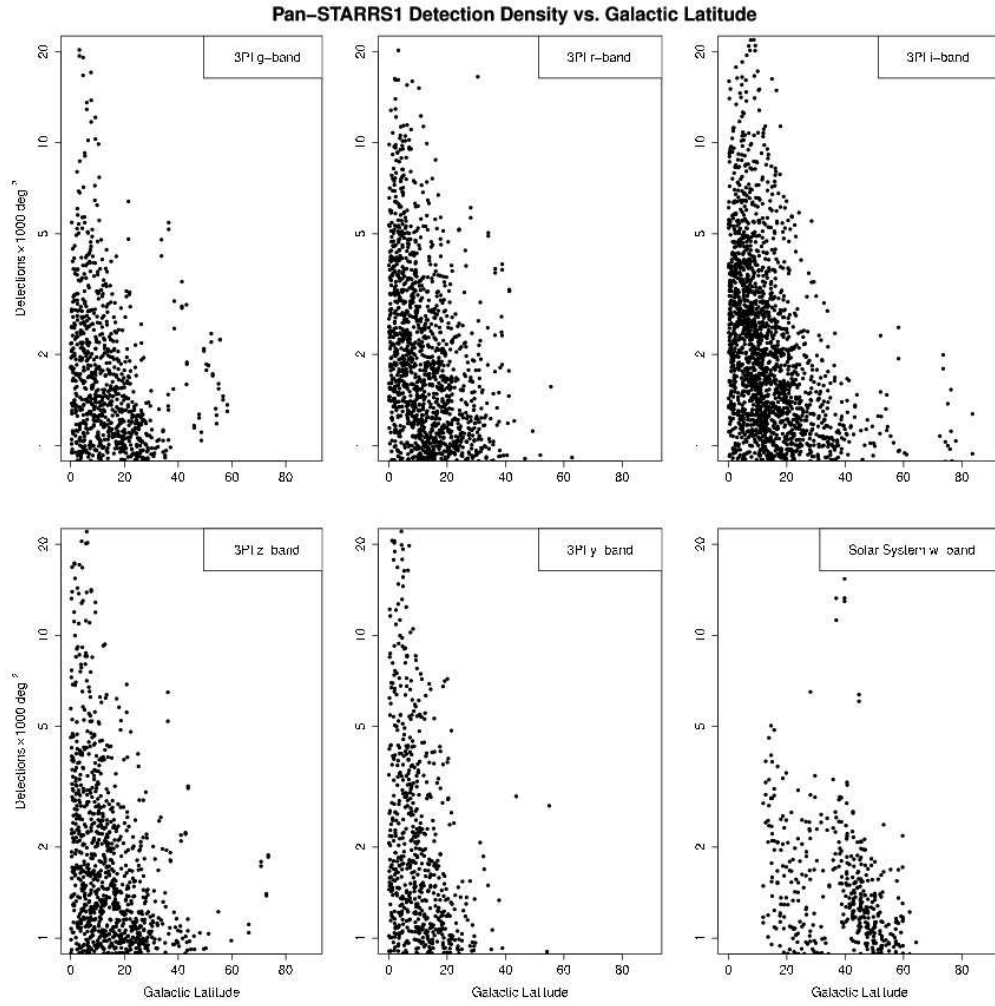


Fig. 15.— Number of transient detections reported to the MOPS by the IPP as a function of galactic latitude in all six Pan-STARRS1 filters. Almost all the transient detections are false.

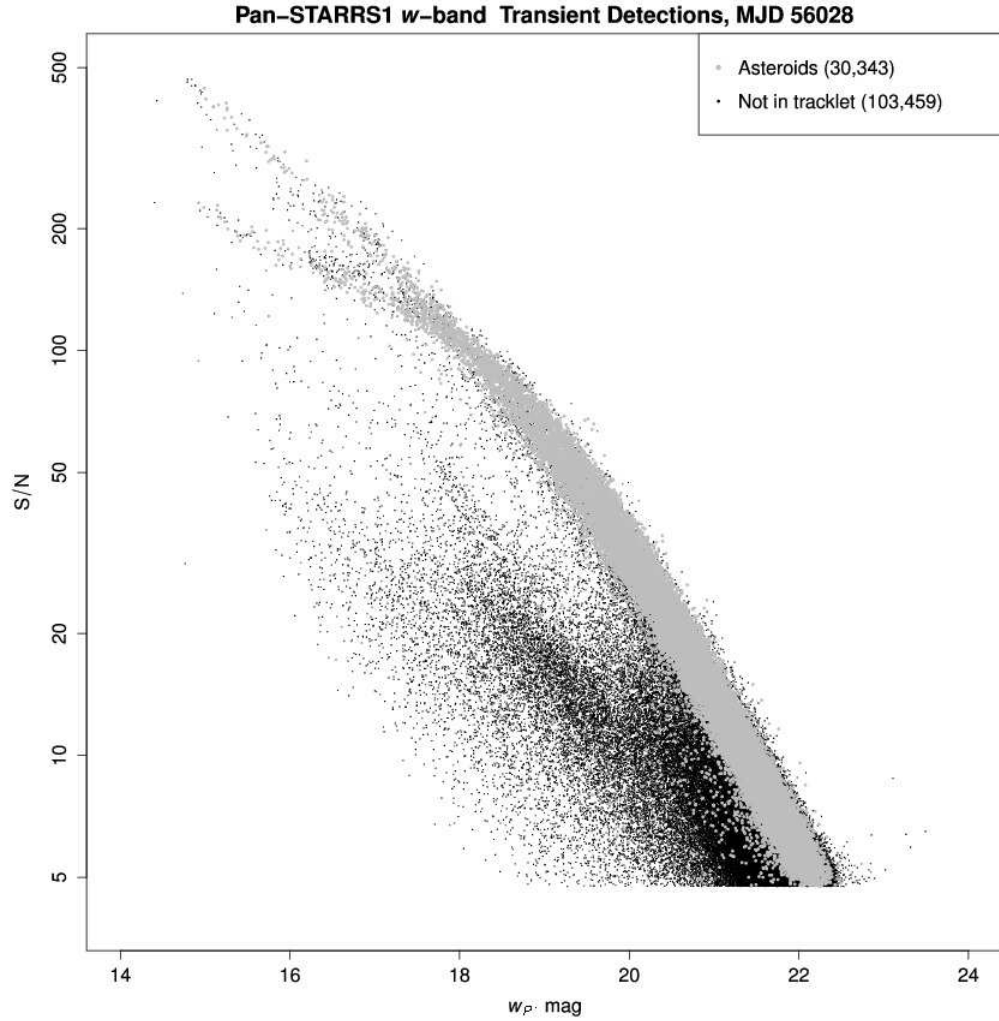


Fig. 16.— Pan-STARRS1 transient detections reported to MOPS by the IPP as a function of  $S/N$  and  $w_{P1}$  magnitude on MJD 56028. Grey dots are detections in tracklets that are real asteroids. Black dots are all other detections. The ‘fork’ in the distribution at  $w_{P1} \sim 18$  is due to a change in observing conditions that caused distortion of PSFs for bright objects.



### Pan-STARRS1 Systematic False Detection Gallery

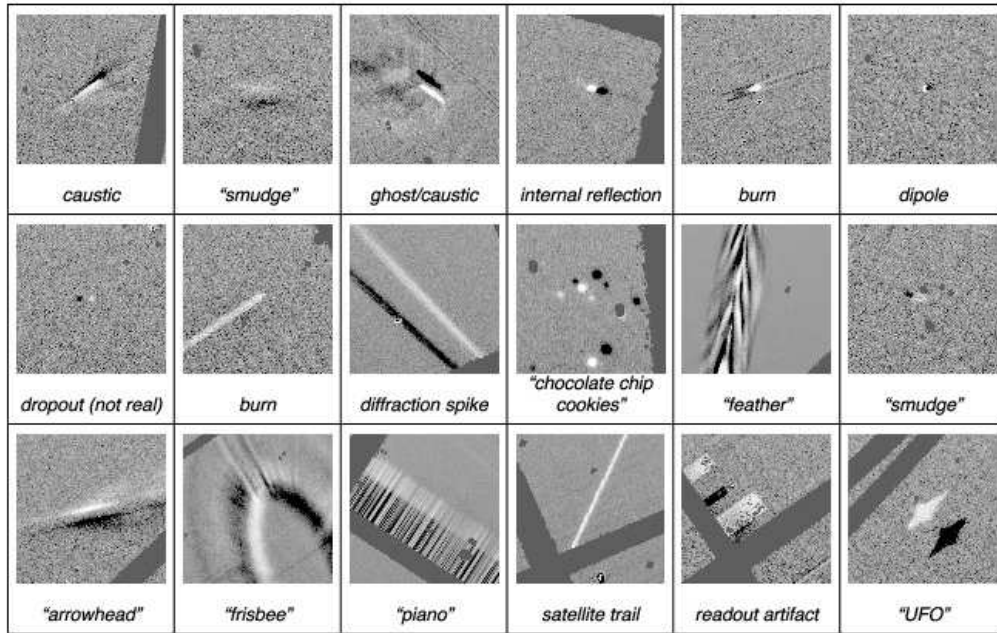


Fig. 17.— A sample of false source detections delivered to MOPS. The cause of the detection is provided under the image when known. The source detections are in the positive image (white pixels). Each image is a  $200 \times 200$  pixel difference image with the original source detection in the center. *i.e.* the difference between two successive images acquired at the same boresight. Solid dark grey regions represent gaps between CCDs or cells or masked regions.

### Pan-STARRS1 Object Detection Gallery

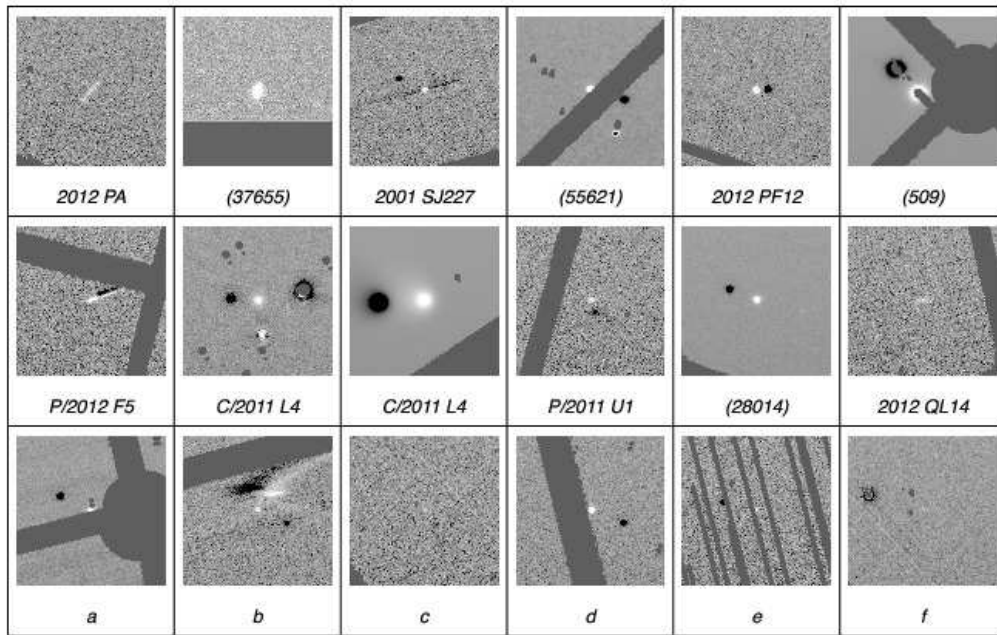


Fig. 18.— A sample of real object detections delivered to MOPS via difference imaging. Each image is a  $200 \times 200$  pixel difference image with the positive source detection in the center. Many detections lie near artifacts or in heavily masked regions or are difficult to distinguish from systematic false detections. Objects *a* through *f* are unknown asteroids. Solid dark grey regions represent gaps between CCDs or cells or masked regions.

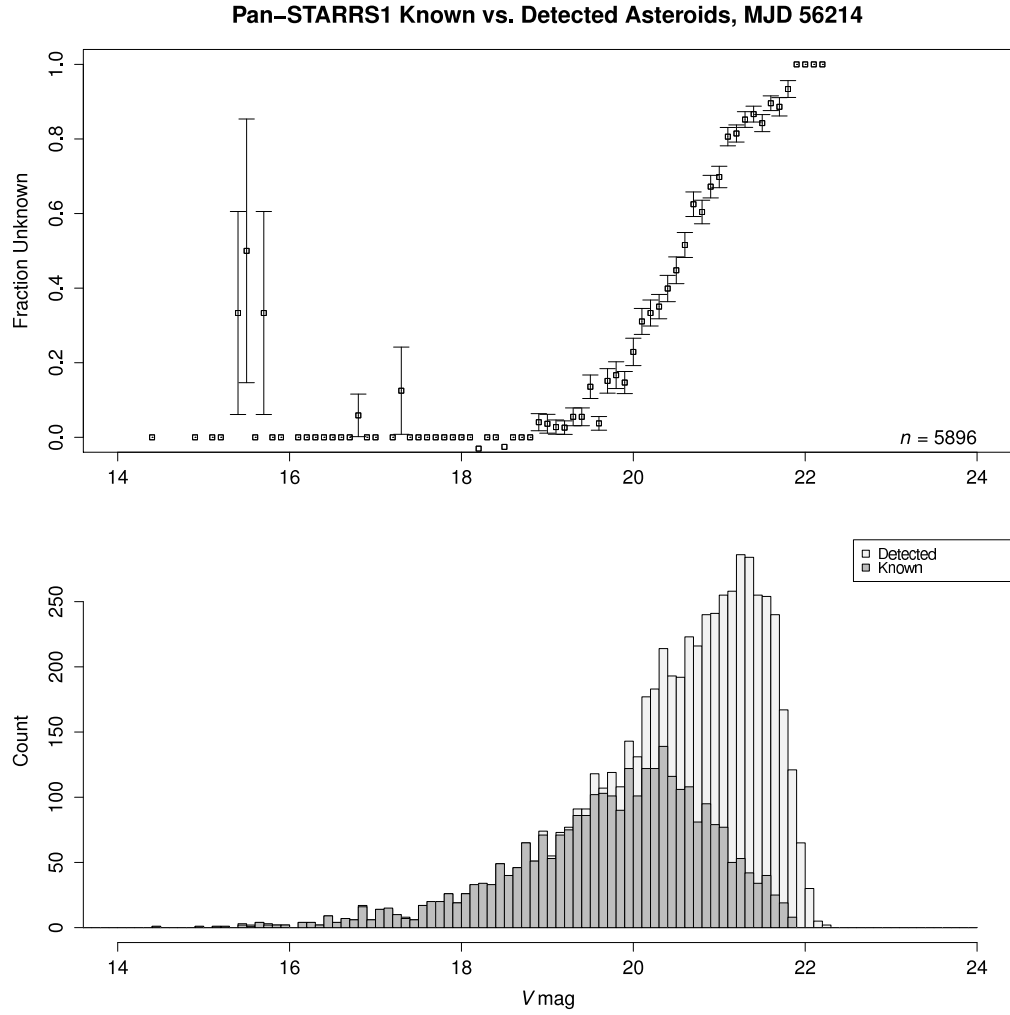


Fig. 19.— Overlapping detected and known asteroid distributions for a single night of Pan-STARRS1 solar system observing.

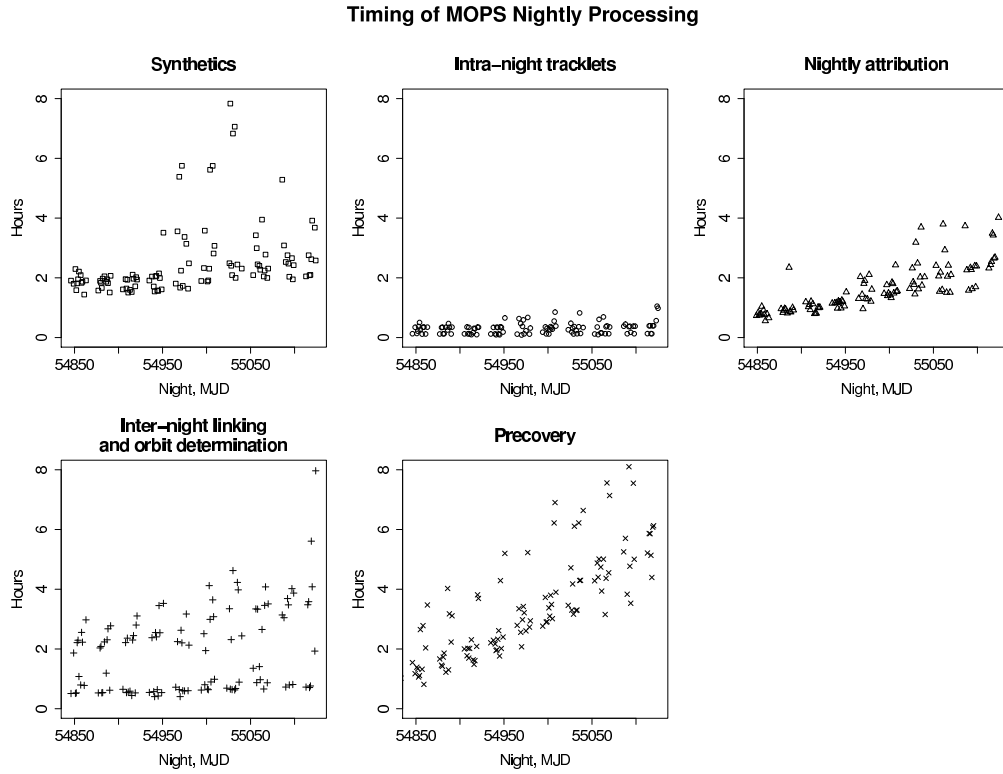


Fig. 20.— Processing times for different MOPS pipeline stages over one simulated year of a two-year simulation using Pan-STARRS4 data volumes. Some data prior to MJD 54850 was discarded because MOPS pipeline software was not separating processing times for synthetic and tracklet stages.

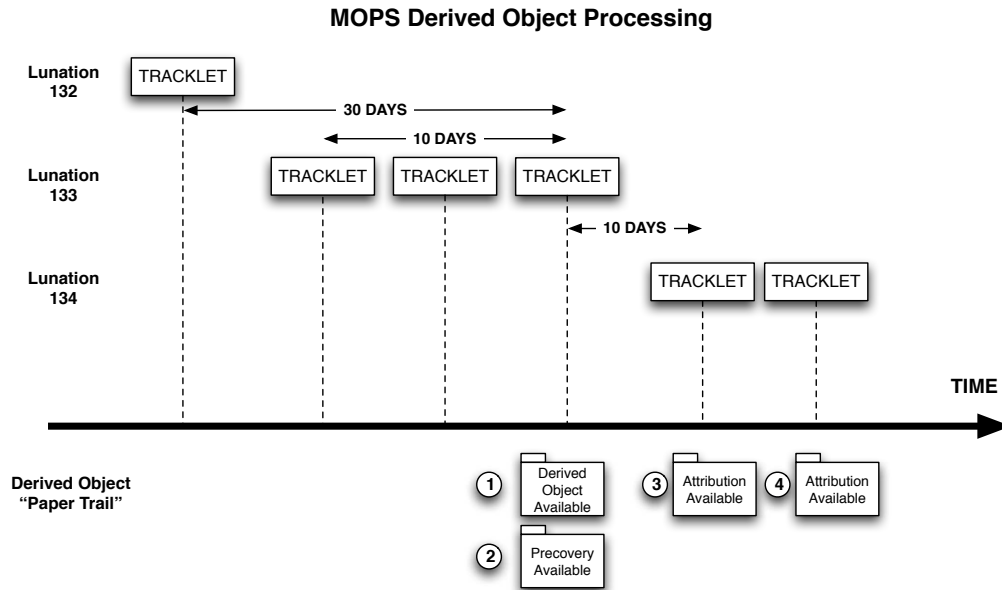


Fig. 21.— MOPS derived object processing overview for a single hypothetical asteroid, showing observed tracklets and the created derived object. In lunation 132, no derivation is available because there is only a single tracklet observed. In lunation 133, three tracklets are observed in a 10 day window, so a derived object is created and the precovery in lunation 132 becomes available. In lunation 134, two attributions are available using predictions from the object's derived orbit. Numbers in circles show the sequence of 'paper trail' records inserted into the MOPS database.

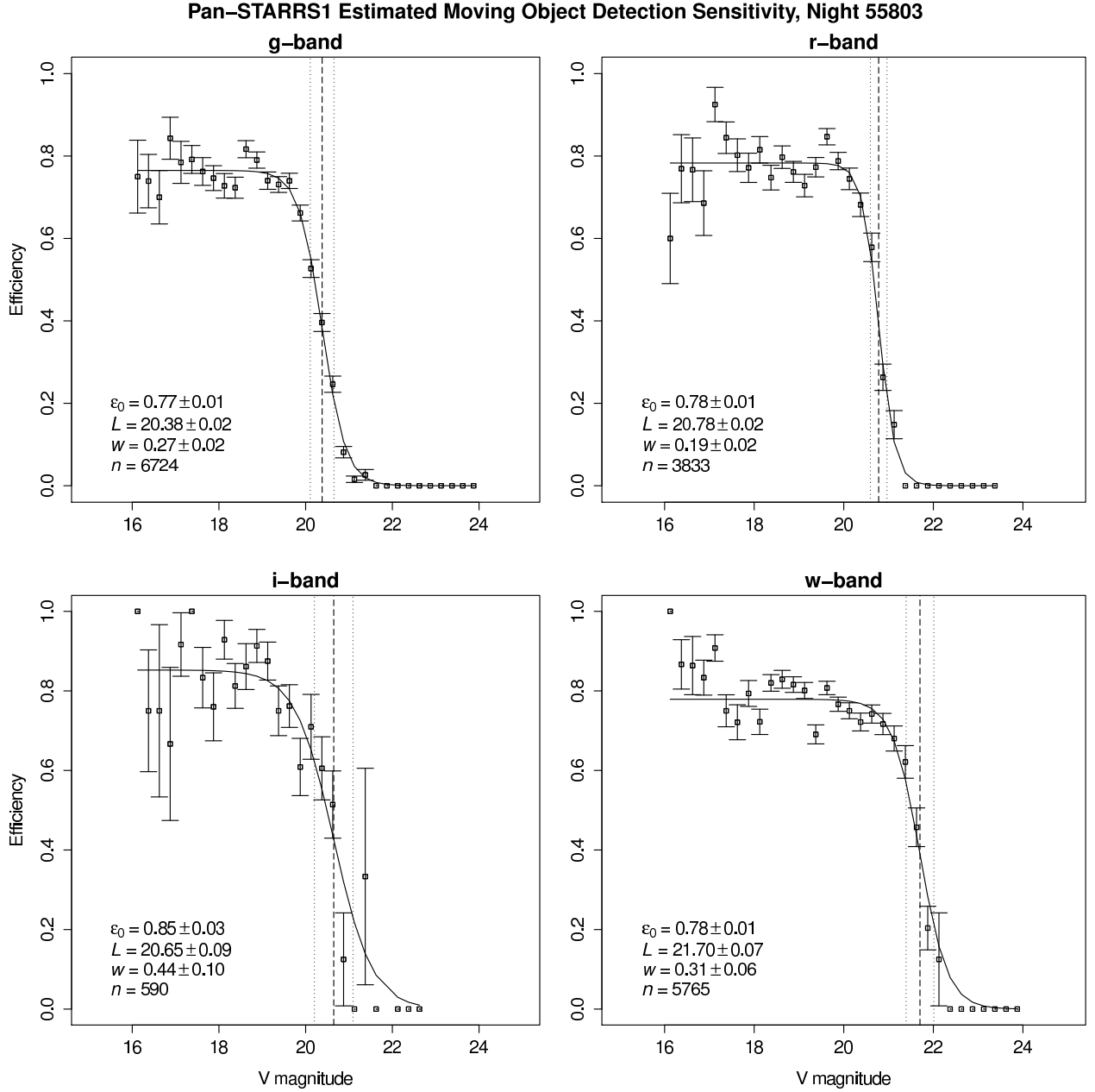


Fig. 22.— Pan-STARRS1 moving object detection efficiency on a single night (MJD 55803) for detections of known numbered and multi-opposition asteroids in each filter as a function of  $V$  magnitude. The data in each filter were fit to the function  $\epsilon = \epsilon_0 \left[ 1 + \exp \left( [V - L]/w \right) \right]^{-1}$  as described in §5.13. The vertical dashed line is at the  $V$  magnitude where the efficiency drops to 50% of the maximum ( $L$ ). The vertical dotted lines provide the range  $[L - w, L + w]$  over which the efficiency drops quickly.

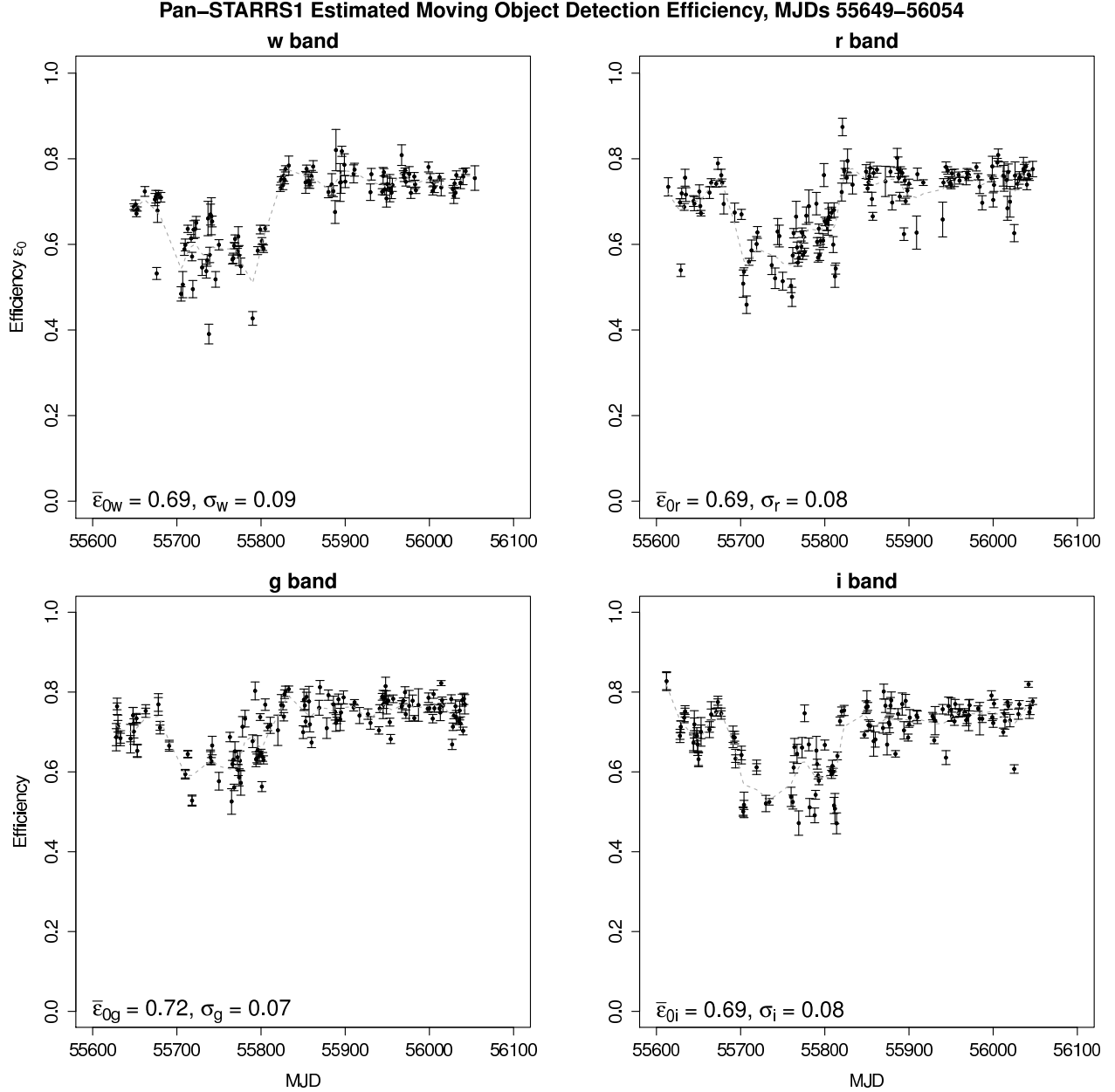


Fig. 23.— Pan-STARRS1 moving object detection efficiency for bright non-saturated detections as a function of MJD corresponding to the time period from approximately Feb 2011 through Jun 2012. Around MJD 55820, MOPS began employing less-aggressive false detection filtering of IPP transient detections, boosting per-exposure detection efficiency to 75% consistently. The dashed line is a spline-fit to the data.

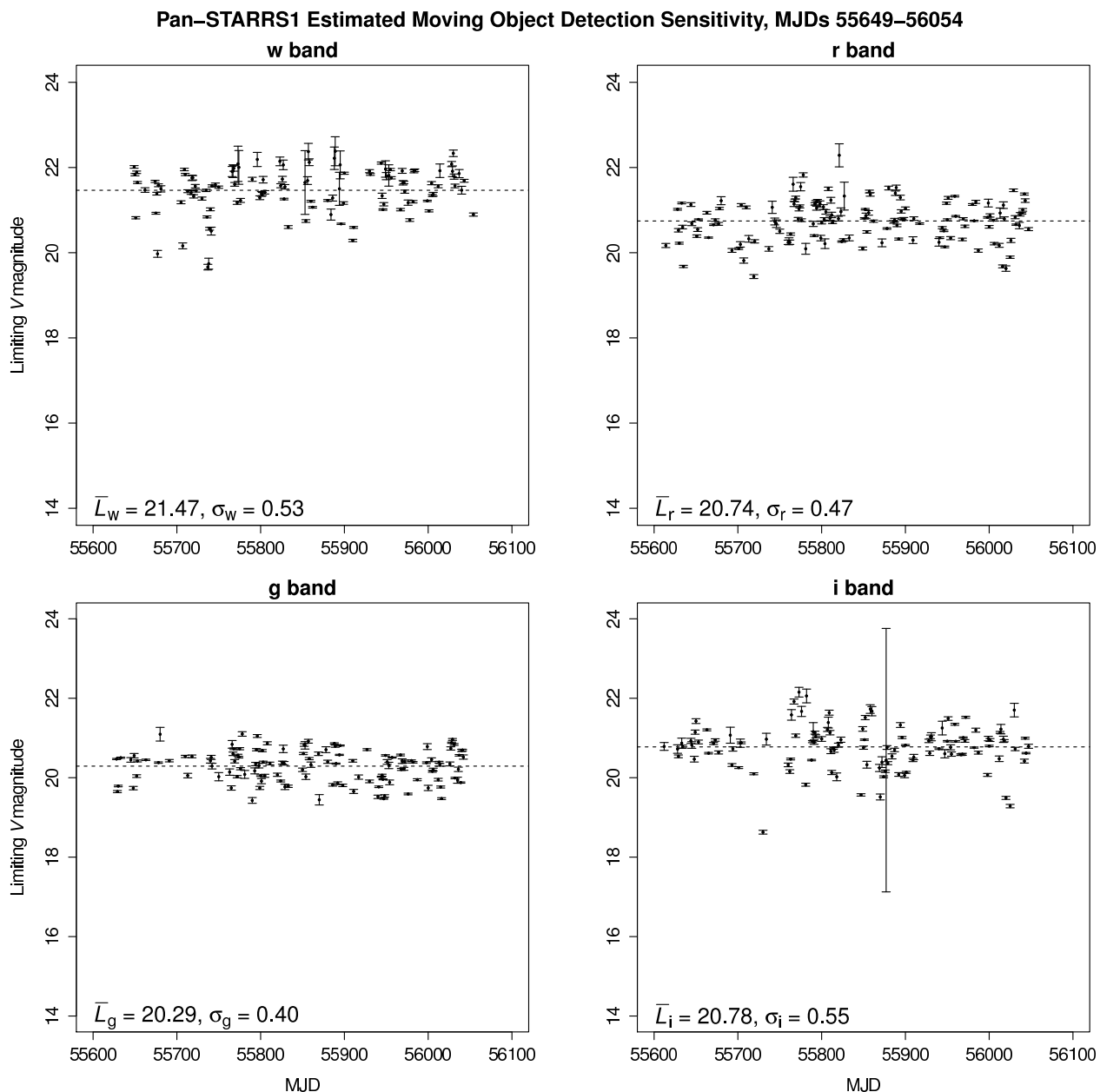


Fig. 24.— Pan-STARRS1 nightly limiting  $V$  magnitude in each of the four main filters used to detect moving objects as a function of MJD corresponding to the time period from approximately Feb 2011 through Jun 2012. The dashed lines represent fits to the passband data as a function of time.



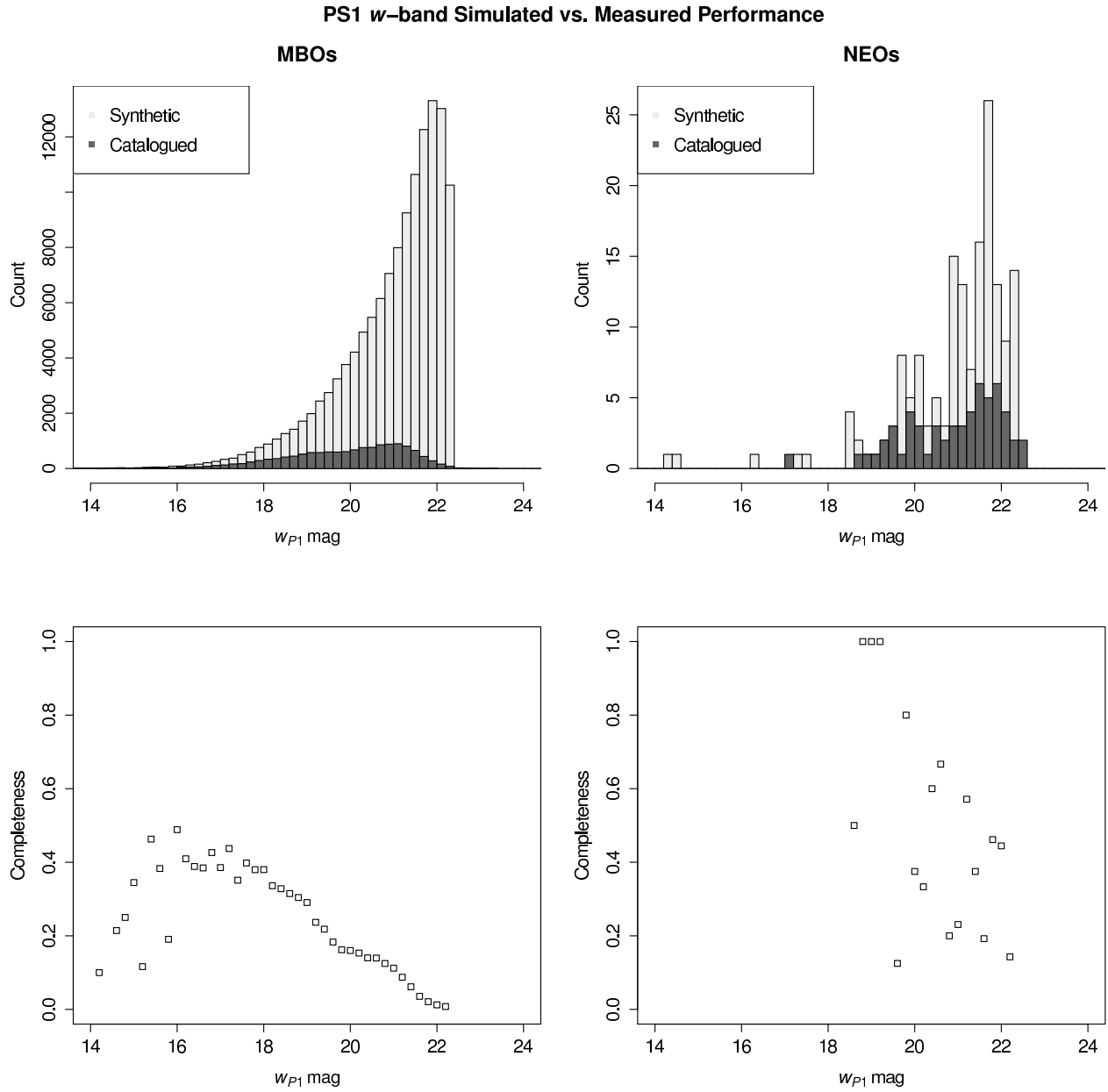


Fig. 25.— Comparison of MOPS synthetic tracklet counts to Pan-STARRS1 submitted tracklets during the period 13 Aug 2011 through 11 Oct 2011 for (left) main belt objects and (right) near-Earth objects.

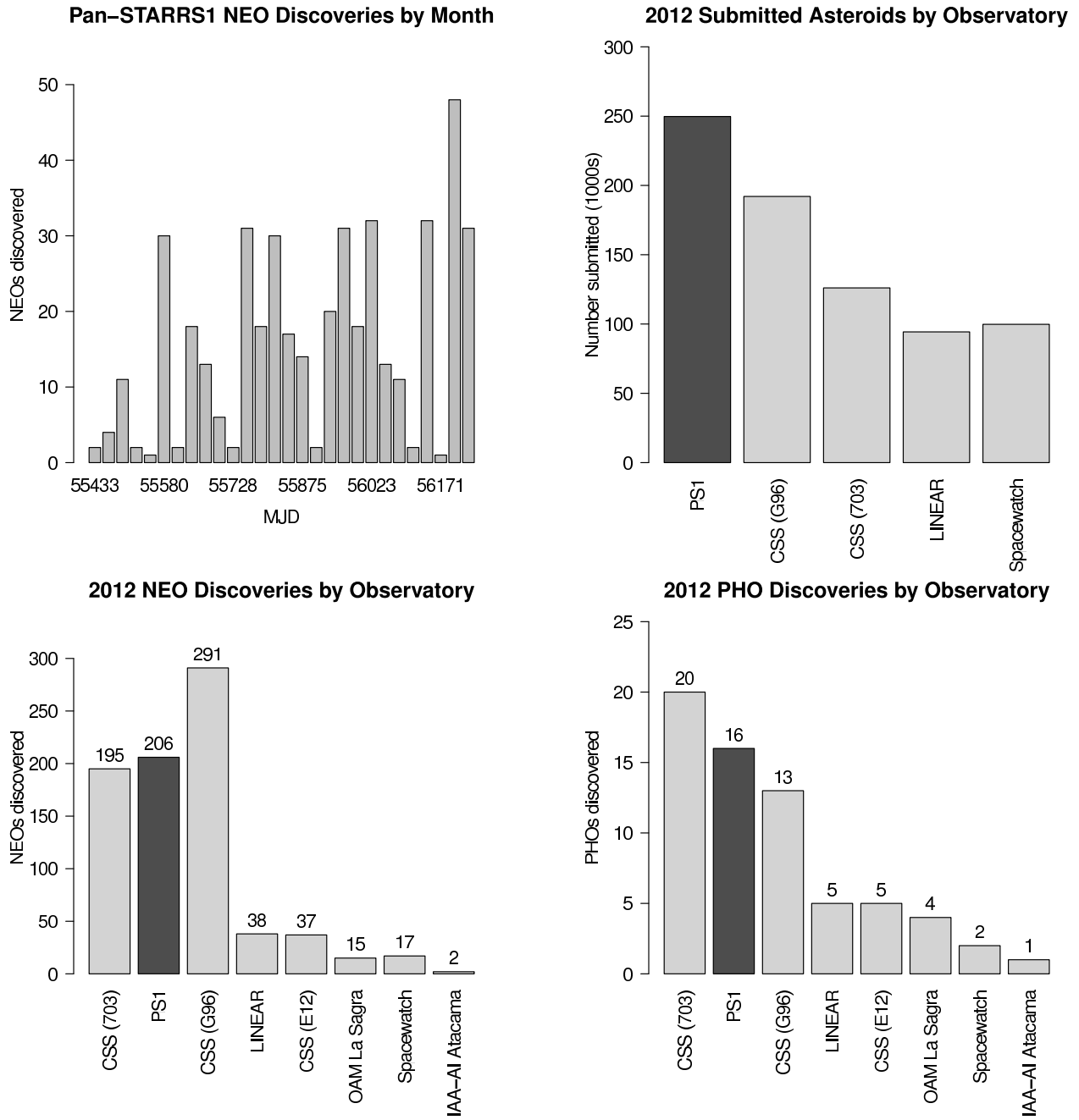


Fig. 26.— Pan-STARRS1 discovery statistics as of November 2012 (from the Minor Planet Center).

## REFERENCES

- Alvarez, L. W., Alvarez, W., Asaro, F., and Michel, H. V. 1980, *Science*, 208, 1095
- Boattini, A. et al. 2009, in *AAS/Division for Planetary Sciences Meeting Abstracts*, Vol. 41, *AAS/Division for Planetary Sciences Meeting Abstracts #41*
- Bowell, E., Koehn, B. W., Howell, S. B., Hoffman, M., and Muinonen, K. 1995, in *Bulletin of the American Astronomical Society*, Vol. 27, *Bulletin of the American Astronomical Society*, p. 1057
- Burgett, W. S. 2012, in *Society of Photo-Optical Instrumentation Engineers (SPIE) Conference Series*, Vol. 8449, *Society of Photo-Optical Instrumentation Engineers (SPIE) Conference Series*
- Chambers, K. 2006, in *The Advanced Maui Optical and Space Surveillance Technologies Conference*
- Chambers, K. C. 2007, in *Bulletin of the American Astronomical Society*, Vol. 39, *American Astronomical Society Meeting Abstracts*, p. #142.06
- Chambers, K. C. 2012, in *American Astronomical Society Meeting Abstracts*, Vol. 220, *American Astronomical Society Meeting Abstracts #220*, p. #107.04
- Chesley, S. R. and Spahr, T. B. 2004, in *Mitigation of Hazardous Comets and Asteroids*, ed. M. J. S. Belton, T. H. Morgan, N. H. Samarasinha, & D. K. Yeomans , p. 22
- Donalek, C., Mahabal, A., Djorgovski, S. G., Marney, S., Drake, A., Glikman, E., Graham, M. J., and Williams, R. 2008, in *American Institute of Physics Conference Series*, Vol. 1082, *American Institute of Physics Conference Series*, ed. C. A. L. Bailer-Jones, p. 252

- Gehrels, T. 1991, *Space Science Reviews*, 58, 347
- Gehrels, T. and Jedicke, R. 1996, *Earth Moon and Planets*, 72, 233
- Gladman, B., Michel, P., and Froeschlé, C. 2000, *Icarus*, 146, 176
- Gladman, B. J. et al. 2009, *Icarus*, 202, 104
- Granvik, M. and Muinonen, K. 2008, *Icarus*, 198, 130
- Granvik, M., Virtanen, J., Oszkiewicz, D., and Muinonen, K. 2009, *Meteoritics and Planetary Science*, 44, 1853
- Grav, T., Jedicke, R., Denneau, L., Chesley, S., Holman, M. J., and Spahr, T. B. 2011, *PASP*, 123, 423
- Harris, A. 2008, *Nature*, 453, 1178
- Helin, E. F., Pravdo, S. H., Rabinowitz, D. L., and Lawrence, K. J. 1997, *New York Academy Sciences Annals*, 822, 6
- Hodapp, K. W. et al. 2004, *Astronomische Nachrichten*, 325, 636
- Jedicke, R. 1996, *AJ*, 111, 970
- Jedicke, R. and Herron, J. D. 1997, *Icarus*, 127, 494
- Jedicke, R., Larsen, J., and Spahr, T. 2002, *Asteroids III*, 71
- Jedicke, R. and Metcalfe, T. S. 1998, *Icarus*, 131, 245
- Jedicke, R., Morbidelli, A., Spahr, T., Petit, J. M., and Bottke, W. F. 2003, *Icarus*, 161, 17
- Jenniskens, P. et al. 2009, *Nature*, 458, 485

- Kaiser, N. 2004, in Society of Photo-Optical Instrumentation Engineers (SPIE) Conference Series, Vol. 5489, Society of Photo-Optical Instrumentation Engineers (SPIE) Conference Series, ed. J. M. Oschmann, Jr., p. 11
- Kaiser, N. et al. 2002, in Society of Photo-Optical Instrumentation Engineers (SPIE) Conference Series, Vol. 4836, Society of Photo-Optical Instrumentation Engineers (SPIE) Conference Series, ed. J. A. Tyson and S. Wolff, p. 154
- Karaali, S., Bilir, S., and Tunçel, S. 2005, PASA, 22, 24
- Kubica, J. et al. 2007, Icarus, 189, 151
- Kubica, J., Moore, A., Connolly, A., and Jedicke, R. 2005, in Proc. SPIE Signal and Data Processing of Small Targets, ed. O. E. Drummond (SPIE)
- Kuiper, G. P., Fujita, Y., Gehrels, T., Groeneveld, I., Kent, J., van Biesbroeck, G., and van Houten, C. J. 1958, ApJS, 3, 289
- Larsen, J. A. et al. 2001, AJ, 121, 562
- Larsen, J. A. et al. 2007, AJ, 133, 1247
- Larson, S. 2007, in IAU Symposium, Vol. 236, IAU Symposium, ed. G. B. Valsecchi and D. Vokrouhlický, p. 323
- Magnier, E. 2006, in The Advanced Maui Optical and Space Surveillance Technologies Conference
- Magnier, E. A., Liu, M., Monet, D. G., and Chambers, K. C. 2008, in IAU Symposium, Vol. 248, IAU Symposium, ed. W. J. Jin, I. Platais, and M. A. C. Perryman, p. 553
- Mainzer, A. et al. 2011, ApJ, 743, 156

- Masiero, J., Jedicke, R., Ďurech, J., Gwyn, S., Denneau, L., and Larsen, J. 2009, *Icarus*, 204, 145
- McMillan, R. S. 2007, in *IAU Symposium*, Vol. 236, *IAU Symposium*, ed. G. B. Valsecchi, D. Vokrouhlický, and A. Milani, p. 329
- Milani, A. and Gronchi, G. F. 2010, *Theory of Orbital Determination* (Cambridge University Press)
- Milani, A., Gronchi, G. F., Farnocchia, D., Knežević, Z., Jedicke, R., Denneau, L., and Pierfederici, F. 2008, *Icarus*, 195, 474
- Milani, A., Gronchi, G. F., Knežević, Z., Sansaturio, M. E., and Arratia, O. 2005, *Icarus*, 179, 350
- Milani, A. et al. 2012, *Icarus*, 220, 114
- Morgan, J., Siegmund, W., and Hude, C. 2006, in *The Advanced Maui Optical and Space Surveillance Technologies Conference*
- Petit, J., Holman, M., Scholl, H., Kavelaars, J., and Gladman, B. 2004, *MNRAS*, 347, 471
- Rabinowitz, D. L. 1991, *AJ*, 101, 1518
- Rabinowitz, D. L. 1993, *ApJ*, 407, 412
- Rabinowitz, D. L. et al. 1993, *Nature*, 363, 704
- Schlafly, E. F. et al. 2012, *ApJ*, 756, 158
- Seaman, R. et al. 2011, *ArXiv e-prints*
- Shoemaker, E. M. 1995, *Geophys. Res. Lett.*, 22, 1555

- Stokes, G. H., Evans, J. B., Viggh, H. E. M., Shelly, F. C., and Pearce, E. C. 2000, *Icarus*, 148, 21
- Thain, D., Tannenbaum, T., and Livny, M. 2005, *Concurrency - Practice and Experience*, 17, 323
- Tonry, J., Burke, B. E., and Schechter, P. L. 1997, *PASP*, 109, 1154
- Tonry, J. L., Luppino, G., Kaiser, N., Burke, B. E., and Jacoby, G. H. 2004, in *Astrophysics and Space Science Library*, Vol. 300, *Scientific Detectors for Astronomy, The Beginning of a New Era*, ed. P. Amico, J. W. Beletic, and J. E. Beletic, p. 395
- Tonry, J. L. et al. 2012, *ApJ*, 750, 99
- Tyson, A. and Angel, R. 2001, in *Astronomical Society of the Pacific Conference Series*, Vol. 232, *The New Era of Wide Field Astronomy*, ed. R. Clowes, A. Adamson, & G. Bromage, p. 347
- van Houten, C. J., van Houten-Groeneveld, I., Herget, P., and Gehrels, T. 1970, *A&AS*, 2, 339
- Vereš, P., Jedicke, R., Wainscoat, R., Granvik, M., Chesley, S., Abe, S., Denneau, L., and Grav, T. 2009, *Icarus*, 203, 472
- Zavodny, M., Jedicke, R., Beshore, E. C., Bernardi, F., and Larson, S. 2008, *Icarus*, 198, 284